EVOLUTION OF THE HOFSTADTER BUTTERFLY IN A TUNABLE OPTICAL LATTICE

A THESIS SUBMITTED TO

THE GRADUATE SCHOOL OF ENGINEERING AND SCIENCE

OF BILKENT UNIVERSITY

IN PARTIAL FULFILLMENT OF THE REQUIREMENTS FOR

THE DEGREE OF

MASTER OF SCIENCE

IN

PHYSICS

By

Fırat Yılmaz

August, 2015

EVOLUTION OF THE HOFSTADTER BUTTERFLY IN A TUNABLE OPTICAL LATTICE

By Fırat Yılmaz

August, 2015

We certify that we have read this thesis and that in our opinion it is fully adequate, in scope and in quality, as a thesis for the degree of Master of Science.

Assoc. Dr. M. Özgür Oktel(Advisor)

Prof. Dr. Bayram Tekin

Assist. Prof. Dr. Balazs Hetenyi

Approved for the Graduate School of Engineering and Science:

Prof. Dr. Levent Onural
Director of the Graduate School

ABSTRACT

EVOLUTION OF THE HOFSTADTER BUTTERFLY IN A TUNABLE OPTICAL LATTICE

Fırat Yılmaz
M.S. in Physics
Advisor: Assoc. Dr. M. Özgür Oktel
August, 2015

There are a limited number of exact solutions for quantum mechanical systems. It is critical to obtain solutions for complex systems. One of these unsolved equations was the famous Harpers equation, which was proposed in 1955[1]. It investigates the behavior of a particle in a periodic potential under a uniform magnetic field in two dimensions. Douglas Hofstadter, in 1976, obtained a numerical solution[2] for the first time, discovering a non-trivial energy spectrum as a function of magnetic flux. The spectrum is a fractal structure, the Hofstadter butterfly, and depends purely on the lattice geometry. In other words, primitive lattice vectors and basis vectors determine the fractal energy spectrum under a uniform magnetic field.

The experimental demonstration of such an energy spectrum requires a magnitude of thousands of Teslas magnetic field in the solid state systems since the area of a unit cell is on the order of a few square nanometers. Recently, two main developments in cold atom physics led the way to the realization of the Hofstadter butterfly energy spectrum. The first one as the creation and manipulation of optical lattices. It provides a controllable environment with lattice constants up to a few hundred nanometers, which means the required magnetic field is now within experimental capabilities. The second development is the realization of synthetic gauge fields on optical lattices. One recent development we focus in this thesis is the creation of an adjustable lattice geometry[3].

The self-similar energy spectra for a uniform magnetic field depends purely on the lattice geometry. Recently, the Zurich group presented a unique chance to examine the connection between them. Particularly, we calculate the Hofstadter butterfly for all lattice parameters which can be obtained by the Zurich group[3]. We then investigate the transition of the Hofstadter butterfly from a checkerboard

lattice to a honeycomb lattice, which includes the observation of the change in topological invariants, the Chern numbers of the self-similar energy spectra.

For this purpose, we first present the theoretical building blocks utilized throughout the research. We show the step-by-step procedure to obtain the Hofstadter butterfly, starting from the continuous Hamiltonian and projection onto a tight-binding Hamiltonian. We explicitly demonstrate the butterflies for the square lattice and the honeycomb lattice. Next, we concentrate on the experiment carried out by the Zurich group, and obtain the Hofstadter butterflies for all lattice geometries.

The Hofstadter butterflies are analysed in detail. There are three different regimes. In the first regime the spectrum is formed by two stacked square lattice Hofstadter butterflies separated by a large energy gap. As the optical lattice evolves from the checkerboard to the honeycomb geometry, the second regime begins with the emergence of Dirac points for particular rational magnetic flux values $\Phi = p/q$, where p, q are mutually prime integers. In the third regime infinitely many sequential closings of adjacent bands around zero energy give the honeycomb lattice Hofstadter butterfly as a limit. This closing process can be probed with current setups.

We show that the existence of Dirac points at zero magnetic field does not imply its existence at a finite field. The topological properties of the energy spectrum can change with the applied magnetic field. We calculate the Chern numbers of the major gaps in the spectra and examine the exchange and the transfer of these topological invariants during the evolution of the lattice geometry. An analytic formula to determine the critical value for the emergence of Dirac points around zero energy is obtained in Eq.5.2

Keywords: Hofstadter, Butterfly, Optical Lattice, Evolution.

ÖZET

HOFSTADTER KELEBEĞİNİN AYARLANABİLİR OPTİK ÖRGÜLERDEKİ DEĞİŞİMİ

Fırat Yılmaz
Fizik, Yüksek Lisans
Tez Danışmanı: Assoc. Dr. M. Özgür Oktel
Ağustos, 2015

Kuantum mekaniksel sistemlerde sınırlı sayıda analitik çözüm vardır. Bu çözümler karmaşık sistemlerin yaklaşık çözümleri için önemlidir. Çözülmemiş denklemlemlerinden biri de ünlü Harper denklemidir. Harper denklemi, 2 boyutlu periyodik potansiyel altındaki parçacığın sabit manyetik alan altında davranışını inceler. İlk tam nümerik çözümü Douglas Hofstader elde etmiştir. Manyetik kuantum akışın fonksiyonu olan enerji spekturumu, karmaşık fraktal bir yapı göstermektedir. Bu spekturum Hofstader kelebeğidir ve sadece örgü geometrisine bağlıdır. Diğer bir deyişle, sabit bir manyetik alan altında fraktal enerji spekturumunu, pirimitif örgü vektörleri ve unite vektörleri belirler.

Katı hal fiziğinde, birim hücresinin alanı bir kaç nanometre kare ölçeğinde olduğundan, bu enerji spekturumlarını deneysel olarak gözlemlemek binlerce Tesla büyüklüğünde manyetik alan gerektirmektedir. Son zamanlarda soğuk atom fiziğindeki iki ana gelişme, Hofstadter kelebeğinin gerçekleştirilmesinin yolunu açtı. Birincisi, optik örgülerin yaratılması ve değiştirilebilmesidir. Bu gelişme örgü sabitini bir kaç nanometreden bir kaç yüz nanometreye kadar kontrol edilebilen alan yaratmayı sağlar ve enerji spekturumunu gözlemlemek için gerekli manyetik alan günümüz deneylerinin ulaşabildiği seviyelere iner. İkinci gelişme, sentetik ayar alanlarının optik ağ örgülerinde gerçellenmesidir. Bu tezde odaklandığımız bir gelişme ise ayarlanabilir optik ağ geometrilerinin yaratılmasıdır[L. Tarruell *et al.*, Nature 483, 302305 (2012)].

Sabit manyetik alanlardaki eş-benzer enerji spekturumu sadece ağ geometrisine bağlıdır ve Zürih araştırma grubu bu bağlantıyı incelemek için bir fırsat sunmuştur. Hofstadter kelebeğini, Zürih grubu tarafından elde edilebilen tüm ağ parametreleri için özel olarak hesapladık[3]. Sonrasında dama örgüden bal peteği örgüsüne geçişte Hofstadter kelebeğinin değişimini inceledik ki bu topolojik sabit

Chern sayılarının eş-benzer enerji spekturumlarındaki değişimlerini de içerir.

Bu amaçla, ilk olarak araştırma sürecinde faydalandığımız teorik yapıtaşlarını sunduk. Sürekli Hamiltonian ve sıkı-bağlı Hamiltonian'dan başlayıp basamak basamak Hofstadter kelebeği elde etme sürecini anlattık. Açık olarak kare örgü ve pal peteği örgüsü için kelebekleri ürettik. Sonrasında Zürih grubunca yapılan deneye yoğunlaştık ve tüm ağ parametreleri için Hofstadter kelebeğini elde ettik.

Bu Hofstadter kelebekleri detaylıca incelendi. Üç farklı bölge bulundu. Birinci bölgede spekturum, iki kare örgü Hofstadter kelebeğinin aralarında geniş bir enerji boşluğu olacak şekilde üst üste halinden oluşur. Optik ağ dama geometrisinden pal peteği geometrisine evrilirken Dirac noktalarının manyetik akının rasyonel değerlerinde ortaya çıkmasıyla ikinci bölge başlar. Üçüncü bölge, sıfır enerji seviyesi etrafındaki komşu bantlar başta olmak üzere sonsuz sayıdaki bantın birbiri üzerine kapanmasıyla pal peteği ağının Hofstadter kelebeğine yakınsamasıyla ulaşılır. Bu kapanma süreci günümüz deney aletleriyle aranabilir.

Gösterdik ki manyetik alansız ortamda Dirac noktalarının varlığı sonlu manyetik alanlarda aynı Dirac noktalarının varlığını garanti etmez. Enerji spekturumunun topolojik özellikleri uygulanan manyetik alanla değişebilir. Spekturumdaki ana enerji boşluklarının Chern sayılarını hesapladık ve bu sayıların ağ geometrisinin değişim sürecinde değiş tokuşunu ve iletimini analiz ettik. Denklem 5.2'de görüldüğü gibi, bu süreçte sıfır enerji etrafında ortaya çıkan Dirac noktalarının kritik bir değere göre belirlendiği bir analitik formül belirledik.

Anahtar sözcükler: Hofstadter, Kelebek, Optik Örgü, Değişim, Dönüşüm.

Acknowledgement

I would like to give my deepest gratitudes to one of the two great minds of human history, Sir Isaac Newton. The reasonable disobedients embrace the scientific truth and are the evolutionary future of Homo sapiens sapiens.

My mother Elif, my father Selahattin, my big brother Burak and my handsome brother Suat, you supported me unconditionally, I am thankful to your efforts on me.

My dear professor M.Ö. Oktel and thank you for all your efforts. This work is the outcome of the egneration of collective study, so thank you all my present and futuer colleaguess, friends.

Our work is supported by Trkiye Bilimsel ve Teknolojik Aratrma Kurumu (TÜBİTAK), I would like to show my gratitutes to TÜBİTAK and all people who supported the scientific works by their very taxes.

Contents

List of Figures

List of Tables

Chapter 1

Introduction

This thesis investigates the evolution of the self-similar energy spectra, the Hofstadter butterfly, as the lattice geometry is adiabatically changed. The energy spectra obtained is a numerical solution of the Harper's equation[1] by Douglas Hofstadter[2]. As the Harper's equation describes a single particle subjected to a 2-D periodic potential and a constant magnetic field. The solution has a fractal energy spectrum as a function of magnetic flux by flux quantum. Until the recent developments [3, 4], it was not possible to realize an adjustable and transformable artificial lattice with a uniform magnetic field. Within the current capabilities, we can analyse how the fractal energy spectra differ from a one particular butterfly to another.

The organization of the thesis is as follows: There are six chapters including "Introduction" and "Conclusion and Future Work" parts. In the Motivation chapter, we discuss the two dimensional optical lattice systems and their potential for the observation of the Hofstadter butterfly. We give a brief summary of the history of the theoretical and the experimental developments in the self-similar energy spectral literature.

In chapter Three, the Hofstadter butterfly is presented and discussed in detail. The calculation procedure of a Hofstadter butterfly for a general lattice

with specific methods are explained. For this purpose, we present the square and the honeycomb lattice geometries, and obtain the corresponding Hofstadter butterflies. The general properties of the two spectra are shown.

In chapter Four, the calculations of the evolution of the Hofstadter butterfly are presented. The numerical solutions of the energy values within a Brillouin zone for the tunable optical lattice parameters are obtained. These energy values are utilized to calculate the tunneling amplitudes for the tight binding approximation by projection into the lowest two bands. The lattice geometry adiabatically transforms from the checkerboard to the honeycomb geometry with an adiabatic change of the basis vectors, so do the corresponding hopping amplitudes. We give a generic method to calculate the butterfly and obtain the spectra to be discussed and analysed in chapter five.

There are two sections in Chapter Five. In the first section, we examine the energy spectra and discuss the topological properties for four particular lattice geometries during the transition process. The topological transformation of the Hofstadter butterfly from the checkerboard to the honeycomb geometry is non-trivial. We find an analytical formula characterizing the topological transition process. There are three topologically distinct parameter regimes. In the second section, we analyze and display the topological change by calculating the first Chern numbers of energy gaps during the adiabatic transition.

In the last chapter, we summarize our results and discuss possible extensions in order to complete the picture for topological transitions as the lattice geometry evolves.

Chapter 2

Motivation

The recent findings and developments in cold atom physics led the investigation of various discoveries in an isolated environment. Two dimensional optical lattices become one of the main focus areas of research due to the defect-free and controllable environment. As the temperature of the system decreases, it becomes possible to investigate properties dominant in low-energy physics such as the emergence of Dirac cones, superconducting Cooper pairs and other interesting phenomena. One interesting theoretical finding in solid state physics is the self-similar energy structure, the Hofstadter butterfly. Douglas Hofstadter investigated the behaviour of an electron under a periodic potential with a uniform magnetic field. Using a tight binding model and imposing Bloch's theorem, he discovered a fractal energy graph as a function of magnetic flux in 1976[2]. This fractal spectrum is a measure-zero Cantor set. In other words, the whole pattern consists of only self-similar gaps [2]. Another exciting property is that the self-similarity is closely related to number theory, namely the Farey sequence[5].

It is, however, difficult to observe this energy spectrum in solid state systems because it is a function of magnetic flux per flux quanta,ϕ/ϕ_0. It requires magnitude of thousands of Tesla magnetic field to scan all flux values since a typical solid state unit cell area is in the order of a few square nanometers. ϕ_0 is the single magnetic flux quantum, and ϕ is defined as the number of magnetic flux

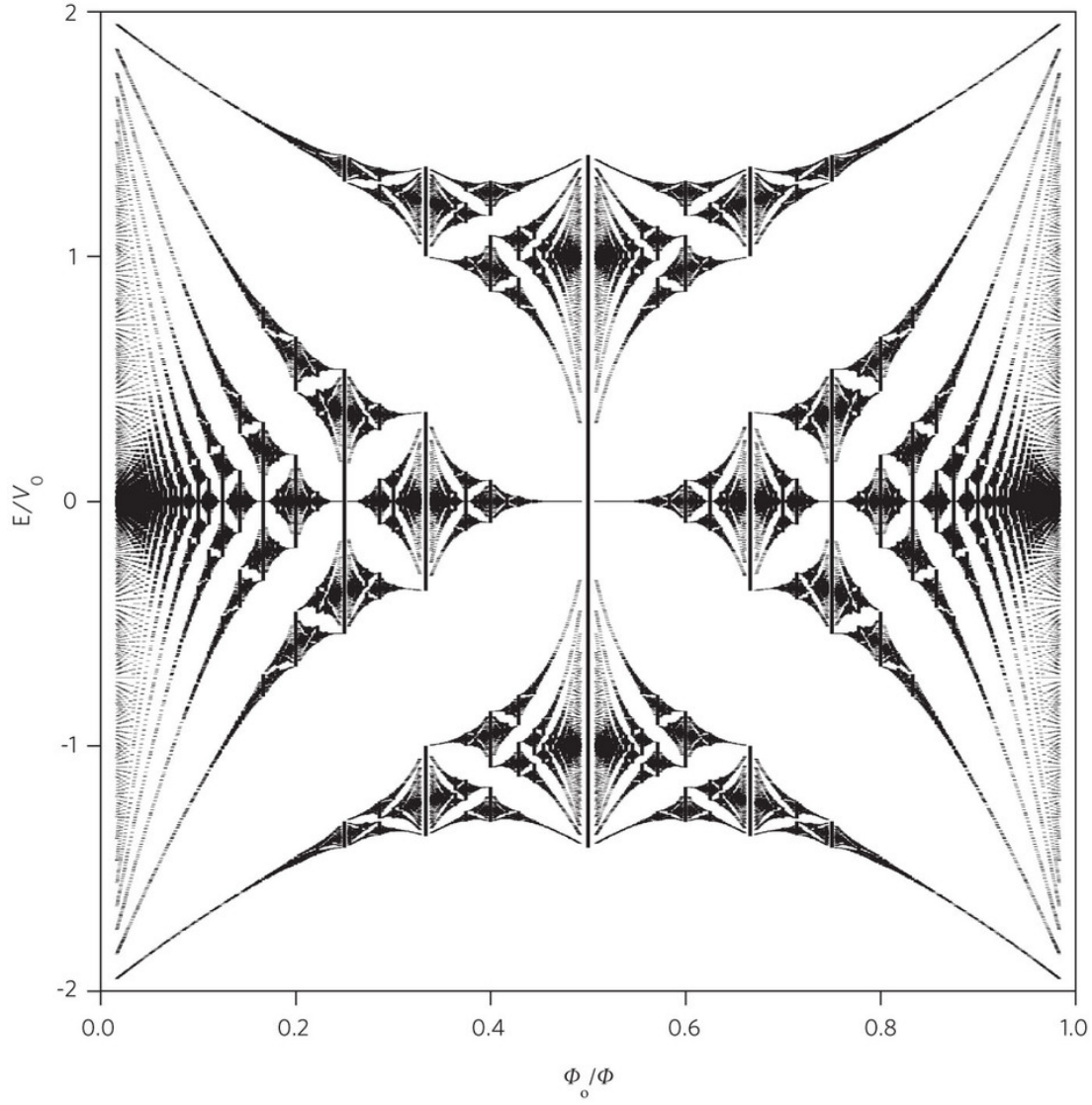

Figure 2.1: Hofstadter butterfly of a square lattice discovered by Douglas Hofstadter in 1976.

quanta trapped in a unit cell. A typical solid state lattice length for a periodic potential is tens of times smaller than the magnetic length at one Tesla. The magnetic length is proportional to the square root of magnetic field while the area that the magnetic field is trapped grows quadratically as the lattice length is increased. If the area of a unit cell is enlarged, it is possible to scan the flux values. This is now achievable with the current magnetic fields.

Recent advances in condensed matter physics and optics allow scientists to investigate the Hofstadter butterfly. The first initiatives to realize the spectra utilized superlattices so that the lattice constant is enlarged and becomes comparable with the magnetic length[6, 7, 8]. These setups, however, lack the adjustability of lattice geometry, types and amount of particles, and types of interactions predominant in the system. The cold atom systems, on the other hand, are capable of offering various lattice geometries formed with different types of particles, controllable interactions and a defect-free environment.

There are two main developments in pursuing fractal energy spectra with cold atoms.

The first one is the generation of artificial effective magnetic fields with a technique called laser assisted tunneling [9, 10]. This allows experimentalists to control the phase of the Fourier decomposed Bloch waves. This method can be used to realize the effect of the magnetic field with the Peierls substitution[11].

The second headway is the development of an adjustable optical lattice[3, 12, 13, 14]. The Zurich group created an optical lattice which can adiabatically change its geometry, namely from triangle to dimer, dimer to honeycomb and other lattice geometries. They recently include an artificial gauge field [4] on top of the experimental setup and realize the Haldane model [15]. Similarly, a uniform magnetic field can be generated on this system as well. Therefore, these two findings let us investigate the fractal nature of the energy spectra of degenerate gases.

Combination of an adjustable lattice with a uniform magnetic field brings new

questions to mind. Two significant questions can be how the relation between topological properties and the lattice geometry is, how the self similar energy spectra do change if the lattice geometry transform from one to another. This thesis aims to answer these two questions. However, it does not aim to explain how the optical lattice is generated, how cold atoms are prepared or how the band mapping technique is realized. We investigate how the Hofstadter butterfly evolves as the lattice parameters are changed.

Our research starts with the analysis of different Hofstadter butterflies and the topological nature of various lattice geometries that can be generated by the Zurich group[3]. Then, we investigate the transition from the checkerboard lattice to the honeycomb lattice geometry through energy spectra and Chern number exchange.

Chapter 3

The Hofstadter Butterfly

The Hofstadter butterfly is a self-similar or fractal energy structure due to the magnetic flux enclosed by a unit cell. It is fully dependent upon the lattice geometry and the applied external field. In other words, the Bravais lattice vectors and basis vectors fully describe the energy spectrum with the choice of magnetic vector potential.

In this section, we go through the literature of the self-similar energy spectra and obtain the Hofstadter butterfly for 2-D lattice geometries with a step-by-step procedure. In the first part, we review the Hofstadter butterfly for a square lattice which is a Bravais lattice. Next, we obtain the Hofstadter butterfly for the triangular lattice with a two point basis, namely the honeycomb lattice.

The preliminary assumptions are as follows,

- A tight-binding model with NN (nearest neighbor) or NNN (next nearest neighbor) hopping is used,

$$\hat{\mathcal{H}} = -\sum_{<<n,m>>} t_{n,m}|n\rangle\langle m|,$$

where $|n\rangle, |m\rangle$ are states localized at two dimensional sites n, m, and t_{nm} is the hopping matrix element between them.

- Landau Gauge is used as the magnetic vector potential,

$$\vec{A} = \big(0, Bx\big),$$

B is the constant magnitude of the magnetic field. - The tunneling amplitudes, $t_{n,m}$, are calculated by fitting to the dispersion relation of the continuum Schrödinger equation. The numerical Schödinger equation is given in Appendix A.

- The effect of the magnetic field is included with Peierls substitution[11],

$$t_{m,n}|\vec{R}_n\rangle\langle\vec{R}_m| \rightarrow e^{-i\Theta_{nm}} t_{m,n}|\vec{R}_n\rangle\langle\vec{R}_m|,$$

and the phase gained is the line integral of the magnetic vector potential along the hopping path.

$$\Theta_{mn} = \frac{q}{\hbar c}\int_{\vec{R}_m}^{\vec{R}_n} \vec{A}\cdot d\vec{\ell},$$

where $|\vec{R}_n\rangle$ and $|\vec{R}_m\rangle$ are the lattice sites. The Peierls substitution is shown to be valid as long as the tight-binding approximation holds at zero magnetic field[16].

- The edge values of the energy bands are important for calculating the Hofstadter butterfly. It is possible to find the critical momentum space points, (k_x, k_y), of band energies for most of the geometries when the magnetic flux by quantum flux is a rational number, $\phi = p/q$. The detailed explanation can be found in litarature[17, 18].

3.1 Bravais Lattice Vectors with One Point Basis

3.1.1 The Square Lattice

The square lattice is a bipartite lattice which makes the band energies symmetric around zero. Each site in a unit cell (site A) is connected with the other site

(site B). Every site has 4 nearest neighbours and the nn tight-binding model captures the single particle system if the potential minima are deep and narrow so that Wannier functions are localized enough. The primitive vectors for the square lattice are,

$$\begin{aligned} \vec{a}_1 &= a\hat{x}, \\ \vec{a}_2 &= a\hat{y}. \end{aligned}$$

a is the lattice constant and the Bravais vectors are $\vec{R}_{m_1,m_2} = m_1 a\hat{x} + m_2 a\hat{y}$ where $(m_1, m_2) \in \mathbb{Z}$.

The nn tight-binding Hamiltonian at zero magnetic field is

$$\begin{aligned} \hat{\mathcal{H}} &= -\sum_{m_1,m_2} \\ &\Big[\quad \epsilon_0 |m_1, m_2\rangle\langle m1, m2| \\ &+ \quad t|m_1+1, m_2\rangle\langle m_1, m_2| \\ &+ \quad t|m_1-1, m_2\rangle\langle m_1, m_2| \\ &+ \quad t|m_1, m_2+1\rangle\langle m_1, m_2| \\ &+ \quad t|m_1, m_2-1\rangle\langle m_1, m_2|\Big]. \end{aligned}$$

We seek eigenstates $\hat{\mathcal{H}}|\Psi\rangle = E|\Psi\rangle$ of the Hamiltonian and which can be expanded as,

$$|\Psi\rangle = \sum_{n_1,n_2} \psi_{n_1,n_2} |n_1, n_2\rangle.$$

and $|n_1, n_2\rangle$ are localized states at lattice sites $n_1, n_2 \in \mathbb{Z}$.

The eigenvalue equation can be written as,

$$\begin{aligned}
\hat{\mathcal{H}}|\Psi\rangle &= E|\Psi\rangle \\
\hat{\mathcal{H}}|\Psi\rangle &= -\sum_{m_1,m_2} \\
&\Big[\ \epsilon_0|m_1,m_2\rangle\langle m_1,m_2| \\
&+ \ t|m_1+1,m_2\rangle\langle m_1,m_2| \\
&+ \ t|m_1-1,m_2\rangle\langle m_1,m_2| \\
&+ \ t|m_1,m_2+1\rangle\langle m_1,m_2| \\
&+ \ t|m_1,m_2-1\rangle\langle m_1,m_2|\Big] \\
&\times \ \sum_{n_1,n_2} \psi_{n_1,n_2}|n_1,n_2\rangle = E\sum_{n_1,n_2} \psi_{n_1,n_2}|n_1,n_2\rangle.
\end{aligned}$$

Projection by $\langle m_1, m_2|$ gives the difference equation:

$$-t\big[\psi_{m_1-1,m_2}+\psi_{m_1+1,m_2}+\psi_{m_1,m_2-1}+\psi_{m_1,m_2+1}\big] = \big(E-\epsilon_0\big)\psi_{m_1,m_2}. \tag{3.1}$$

The Hamiltonian commutes with the translation operator and they do have mutual eigenstates. Separating the wave functions, we can choose the mutual eigenstates as plane waves,

$$\psi_{m_1,m_2} = \psi_0 e^{ik_1m_1}e^{ik_2m_2}.$$

Substituting back into (3.1):

$$\big(E-\epsilon_0\big)\psi_0 e^{ik_1m_1}e^{ik_2m_2} = \psi_0 e^{ik_1m_1}e^{ik_2m_2}\Big[-t\big[e^{-ik_1}+e^{ik_1}+e^{-ik_2}+e^{ik_2}\big]\Big],$$

we can obtain the energy dispersion relation.

$$E(k_1,k_2) = \epsilon_0 - 2t\cos(k_1) - 2t\cos(k_2), \tag{3.2}$$

where $k_1 = \vec{k}\cdot\vec{a_1} = ak_x$, $k_2 = \vec{k}\cdot\vec{a_2} = ak_y$ and $\epsilon_0 = 0$. The first Brillouin zone has square shape as expected (Fig.3.1.1).

Peierls substitution includes the effect of the magnetic field to the system by using complex valued tunneling amplitudes. The Landau Gauge is chosen for uniform magnetic field, $\vec{A} = Bx\hat{y}$.

$$t_{m,n}|\vec{R}_n\rangle\langle\vec{R}_m| \to e^{-i\Theta_{nm}}t_{m,n}|\vec{R}_n\rangle\langle\vec{R}_m|.$$

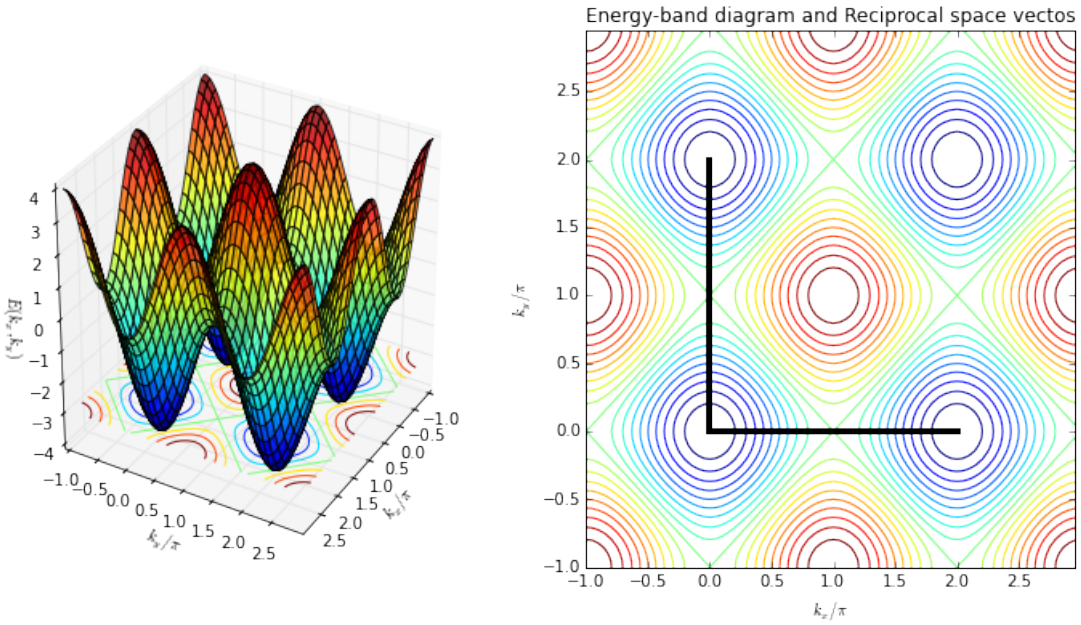

Figure 3.1: Energy-band diagram of the square lattice without magnetic field. The reciprocal lattice vectors are also shown.

The phase is,

$$\begin{aligned}\Theta_{mn} &= \frac{e}{\hbar c}\int_{\vec{R}_{m_1,m_2}}^{\vec{R}_{n_1,n_2}} \vec{A}\cdot d\vec{\ell} \\ &= \pi\Phi\big(\vec{R}_n-\vec{R}_m\big)_y\big(\vec{R}_n+\vec{R}_m\big)_x \\ &= 2\pi\Phi\left(n_2-m_2\right)\left[m_1+\frac{n_1-m_1}{2}\right],\end{aligned}$$

where $\Phi = \phi/\phi_0$, $\phi_0 = hc/e$ is the flux quantum and $\phi = Ba^2$ is the magnetic flux through a unit cell for the square lattice.

The modified nn tight-binding Hamiltonian with a magnetic field is written

as,

$$\begin{aligned}
\hat{\mathcal{H}} &= -\sum_{m_1,m_2} \\
&\Big[\quad \epsilon_0 |m_1, m_2\rangle\langle m_1, m_2| \\
&+ \quad t|m_1+1, m_2\rangle\langle m_1, m_2| \\
&+ \quad t|m_1-1, m_2\rangle\langle m_1, m_2| \\
&+ \quad t|m_1, m_2+1\rangle\langle m_1, m_2| e^{-i2\pi\Phi m_1} \\
&+ \quad t|m_1, m_2-1\rangle\langle m_1, m_2| e^{i2\pi\Phi m_1} \Big].
\end{aligned}$$

Before going into the rest of the calculations for eigenvalue equation and energy diagram, it is a good exercise to calculate the phase gained for a loop around a unit cell.

$[0,0 \to 1,0](\Delta\phi = 0), [1,0 \to 1,1](\Delta\phi = -2\pi\Phi), [1,1 \to 0,1](\Delta\phi = 0), [0,1 \to 0,0](\Delta\phi = 0)$ and the total phase gained around a unit cell is $-2\pi\Phi$. For an integer value of magnetic flux, the phase phase around a unit cell is $-2\pi p/q$

How can we interpret this result? Underlining the very definition of probability distribution function (absolute square of a wave function in Born interpretation), it is uniquely defined over a given domain and single-valued. Moreover, the definition of a unit cell is that the localized wave function on a particular Bravais lattice site repeats itself with a Bloch phase on other sites.

$$\begin{aligned}
\psi(\vec{r} + \vec{R_{m,n}}) &= e^{i\vec{k}\cdot m\vec{a_1}} e^{i\vec{k}\cdot n\vec{a_2}} \psi(\vec{r}) \\
|\psi(\vec{r} + \vec{R_{m,n}})|^2 &= |e^{i\vec{k}\cdot m\vec{a_1}} e^{i\vec{k}\cdot n\vec{a_2}} \psi(\vec{r})|^2 = |\psi(\vec{r})|^2.
\end{aligned}$$

The unit cell at zero magnetic field does not repeat itself with a Bloch phase determined by translation from one site to another. It gains an extra phase due to the applied magnetic field, and the new unit cell must be chosen such that the phase gained does satisfy its definition. From this point of view, we are seeking for a 'magnetic' unit cell, which is uniquely defined on a given domain. In other words, phase gained around this cell must be 2π (or $2\pi n$ where n is an integer) so that phase gained becomes $e^{i2\pi n} = 1$ and the wave function becomes single-valued.

The magnetic unit cell[19] is expanded along the necessary direction provided it is single-valued. If the phase gained for each cell is $\pm 2\pi p/q$, where p and q are mutually prime numbers, the magnetic unit cell must include q-adjacent cells. Then, $2\pi\frac{p}{q}\cdot q = 2\pi p$ gives a self-consistent probability distribution. Consequently, the Brillouin zone is narrowed by the same factor the real space unit-cell expands.

Now going back to calculations, the difference equation can is as follows,

$$-t\big[\psi_{m_1-1,m_2} + \psi_{m_1+1,m_2} + \psi_{m_1,m_2-1}e^{-i2\Phi m_1} + \psi_{m_1,m_2+1}e^{i2\Phi m_1}\big] = \big(E-\epsilon_0\big)\psi_{m_1,m_2}.$$

The eigenvalue equation can be evaluated as,

$$\begin{aligned}
\hat{\mathcal{H}}|\Psi\rangle &= E|\Psi\rangle \\
\hat{\mathcal{H}}|\Psi\rangle &= -\sum_{m_1,m_2} \\
&\Big[\ \epsilon_0|m_1,m_2\rangle\langle m_1,m_2| \\
&+\ t|m_1+1,m_2\rangle\langle m_1,m_2| \\
&+\ t|m_1-1,m_2\rangle\langle m_1,m2| \\
&+\ t|m_1,m_2+1\rangle\langle m_1,m_2|e^{-i2\pi\Phi m_1} \\
&+\ t|m_1,m_2-1\rangle\langle m_1,m_2|e^{i2\pi\Phi m_1}\Big] \\
&\times\ \sum_{n_1,n_2}\psi(n_1,n_2)|n_1,n_2\rangle = E\sum_{n_1,n_2}\psi(n_1,n_2)|n_1,n_2\rangle.
\end{aligned}$$

The difference equation does preserve itself under translations in m_2 with a phase factor. In other words, the Hamiltonian commutes with the translation operator along $\vec{a_2}$ and their eigenstates can be mutually chosen. Therefore, eigenstates can be written as:

$$\psi_{m1,m2} = g_{m_1}e^{ik_2m_2}$$

where $k_1 = \vec{k}\cdot\vec{a_1} = ak_x$ and $k_2 = \vec{k}\cdot\vec{a_2} = ak_y$.

It is necessary to emphasise that, it is a matter of choice how we build our magnetic unit cell. The simpler the choice is, the less likely we make mistakes. Our eigenstates have plane wave behaviour along the direction of the magnetic vector potential in the Landau Gauge, and plane wave part can be separated out.

The resulting difference equation is the Harper's equation.

$$\begin{aligned}(E-\epsilon_0)g_{m_1} &= -t\big[g_{m_1-1}+g_{m_1+1}+g_{m_1}e^{-i(2\pi\Phi m_1+k_2)}+g_{m_1}e^{i(2\pi\Phi m_1+k_2)}\big] \\ &= -t\big[g_{m_1-1}+g_{m_1+1}+g_{m_1}2\cos(2\pi\Phi m_1+k_2)\big].\end{aligned}$$

The rational values of $\Phi = p/q$ makes the equation periodic with q. We take $\epsilon_0 = 0$. Applying Bloch's theorem,

$$g_{-1} = g_{q-1}e^{-iqk_1}, g_q = g_0 e^{iqk_1},$$

and consequently, the system is reduced to q independent equations to be solved mutually. The resulting matrix equation is,

$$-t\big[g_{q-1}e^{-iqk_1}+g_1+g_{m_1}2\cos(2\pi\frac{p}{q}0+k_2)\big] = Eg_0 \tag{3.3}$$

$$-t\big[g_0+g_2+g_1 2\cos(2\pi\frac{p}{q}1+k_2)\big] = Eg_1 \tag{3.4}$$

$$... \tag{3.5}$$

$$-t\big[g_{q-2}+g_0e^{iqk_1}+g_{q-1}2cos(2\pi\frac{p}{q}(q-1)+k_2)\big] = Eg_{q-1}. \tag{3.6}$$

The matrix equation is $W(k_x,k_y)\underline{g}-\underline{\underline{E}}\underline{g}=0$, where $W(k_1,k_2)$ is the corresponding Hamiltonian. The secular determinant of the matrix equation is the characteristic equation of energies for rational $\Phi = p/q$ values. What remains is to solve the characteristic equation for each rational Φ value and form the butterfly energy spectra.

Before going into the calculation of whole energy spectra, it is a good exercise to generate the energy bands for $\Phi = 1/3$ as seen in Fig.3.2. The periodicity of the unit cell becomes $q = 3$. It means the Brillouin zone discontinuously folds onto itself three times and there are three energy bands. The Hofstadter butterfly is calculated by plotting each of the energy eigenvalues for momentum values over the first Brillouin zone. In our system, here are q bands for a particular $\Phi = p/q$ value. If we can determine the critical values k_1^{cri}, k_2^{cri} for the maximum and the minimum values for each energy band, we do not have to calculate energies in between these values. Therefore, we can greatly reduce the computational work, a single line can be drawn between the maximum and the minimum values of each energy band. For this purpose, two papers in Ref.[2, 17] are utilized, where one can find the theoretical procedure to calculate the critical points.

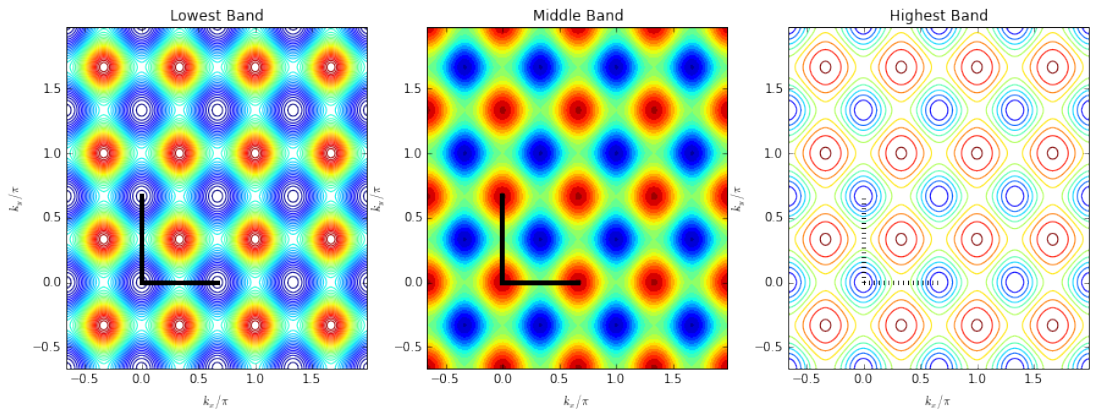

Figure 3.2: Energy-band diagram of Square lattice for $\Phi = 1/3$. The single band is now fractured into $q = 3$ subbands with energy gaps between them. The energy is degenerate the Brillouin zone is becomes $3 \times 3 = 9$ times narrower. The reciprocal lattice vectors are shown accordingly.

The secular determinant obtained from Eq.3.3 is as follows, $D(\lambda, k_1, k_2) \doteq det(W(k_1, k_2) - \lambda I) = 0$. It is a q^{th} order polynomial of λ for each k_1 and k_2 values. The solution of this equation for λ values are energy values obtained for k_1 and k_2 momentum values.

The properties of this characteristic polynomial, $D(\lambda, k_1, k_2)$, are:

$$D(\lambda, k_1, k_2) = D(\lambda, k_1, k_2 + 2\pi/q) = D(\lambda, k_1 + 2\pi/q, k_2).$$

It is periodic along k_1 and k_2 direction with $2\pi/q$. The periodicity in k_2 is due to q-site periodicity in real space, the magnetic unit cell. In addition, the periodicity in k_1 is due to the q-fold degeneracy along the direction k_1.

If we can separate the characteristic polynomial into two parts, $D(\lambda, k_1, k_2) = D_1(\lambda) + D_2(k_1, k_2)$, then the critical points of $D_2(k_1, k_2)$ determines the zeros of $D(\lambda, k_1, k_2)$ since (k_1, k_2) are free parameters in the equation.

$$D_2(k1, k2) = (-1)^{(p+1)q} cos(qk_y) + (-1)^{q+1} cos(qk_x). \tag{3.7}$$

The critical points for Eq.3.7 are easily calculated.

$$\begin{aligned} (k_x, k_y) &= (0, 0) \\ (k_x, k_y) &= (\pi/q, \pi/q). \end{aligned}$$

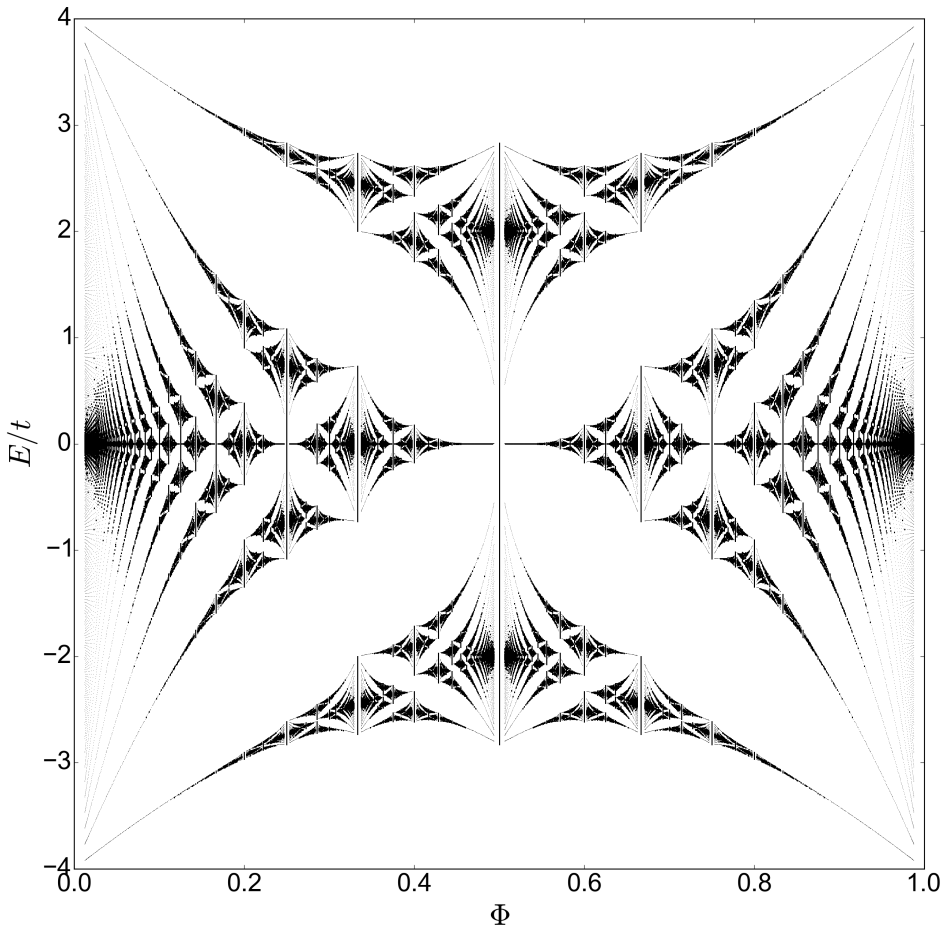

Figure 3.3: Hofstadter butterfly calculated for the Square lattice. Only the critical points are used to obtain the edge energy values, which speed up the calculations dramatically.

We calculate and plot the Hofstadter butterfly for the square lattice. Fig.3.3 shows the butterfly as a function of magnetic flux has self-similar patterns. The main skeleton does repeat itself with small scale deformations. The energy band splits into q bands for $\Phi = p/q$ where p and q are mutually prime numbers. For $\Phi = 1/3$, the main single band splits into 3-subbands, and for $\Phi = 1/33$, it splits into 33-subbands.

An interesting question is what happens when Φ is an irrational number? There is no direct answer for the irrational magnetic flux values since it cannot be solved exactly without periodicity. However, it is possible to anticipate from the butterfly that the main bands split into an infinite number of subbands.

3.2 Bravais Lattice Vectors with Two Point Basis

3.2.1 The Honeycomb Lattice

The honeycomb lattice is a triangle lattice with two sites (A, B) in each unit cell. It is a bipartite lattice, which consists of two sublattices and only the inter-band hopping, $A - B$, $B - A$, are possible. The nn tight binding approximation does exclude $A - A$ and $B - B$ hopping. The primitive vectors forming the Bravais lattice vectors are,

$$\begin{aligned} \vec{a}_1 &= a\sqrt{3}\hat{y} \\ \vec{a}_2 &= a\frac{3}{2}\hat{x} + a\frac{\sqrt{3}}{2}\hat{y}. \end{aligned}$$

The coordinates are chosen such that $\vec{a_2}$ is along y-axis. The Bravais lattice vectors are $\vec{R_{m1,m2}} = m_1\vec{a_1} + m_2\vec{a_2}$, where $(m_1, m_2) \in \mathbb{Z}$. The Hamiltonian without the magnetic field has six nearest neighbors and the energy dispersion

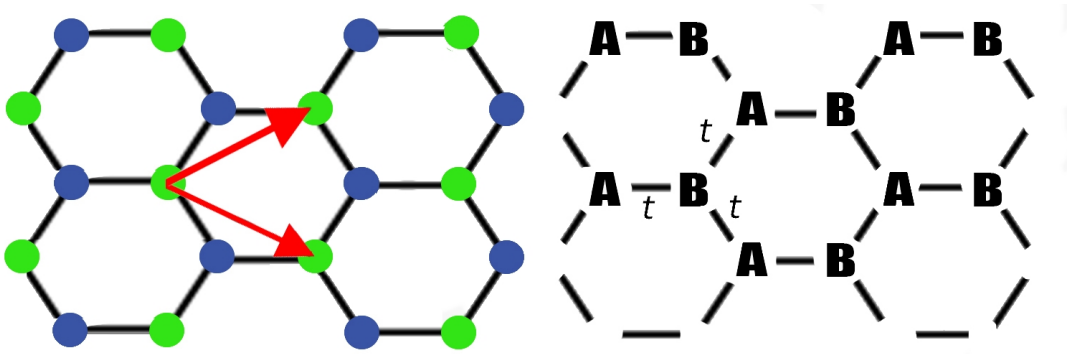

Figure 3.4: Honeycomb lattice geometry with primitive vectors. The hopping amplitudes and sites in each unit cell are illustrated.

relation can be calculated.

$$
\begin{aligned}
\hat{\mathcal{H}}|\Psi\rangle &= \epsilon|\Psi\rangle \\
&= -\sum_{m_1,m_2}\Big[\\
&+ \; t|m_1,m_2,A\rangle\langle m_1,m_2,B| \\
&+ \; t|m_1,m_2,B\rangle\langle m_1,m_2,A| \\
&+ \; t|m_1+1,m_2,A\rangle\langle m_1,m_2,B| \\
&+ \; t|m_1-1,m_2,B\rangle\langle m_1,m_2,A| \\
&+ \; t|m_1,m_2+1,A\rangle\langle m_1,m_2,B| \\
&+ \; t|m_1,m_2-1,B\rangle\langle m_1,m_2,A|\Big] \\
&\times \; \Big[\sum_{n_1,n_2}\psi^A(n_1,n_2)|n_1,n_2,A\rangle + \psi^B(n_1,n_2)|n_1,n_2,B\rangle\Big]
\end{aligned}
$$

Two coupled difference equations are obtained as

$$
\begin{aligned}
\epsilon\psi^B(m_1,m_2) &= \\
&- \; t\Big[\psi^A(m_1,m_2)+\psi^A(m_1+1,m_2)+\psi^A(m_1,m_2+1)\Big] \\
\epsilon\psi^A(m_1,m_2) &= \\
&- \; t\Big[\psi^B(m_1,m_2)+\psi^B(m_1-1,m_2)+\psi^B(m_1,m_2-1)\Big].
\end{aligned}
$$

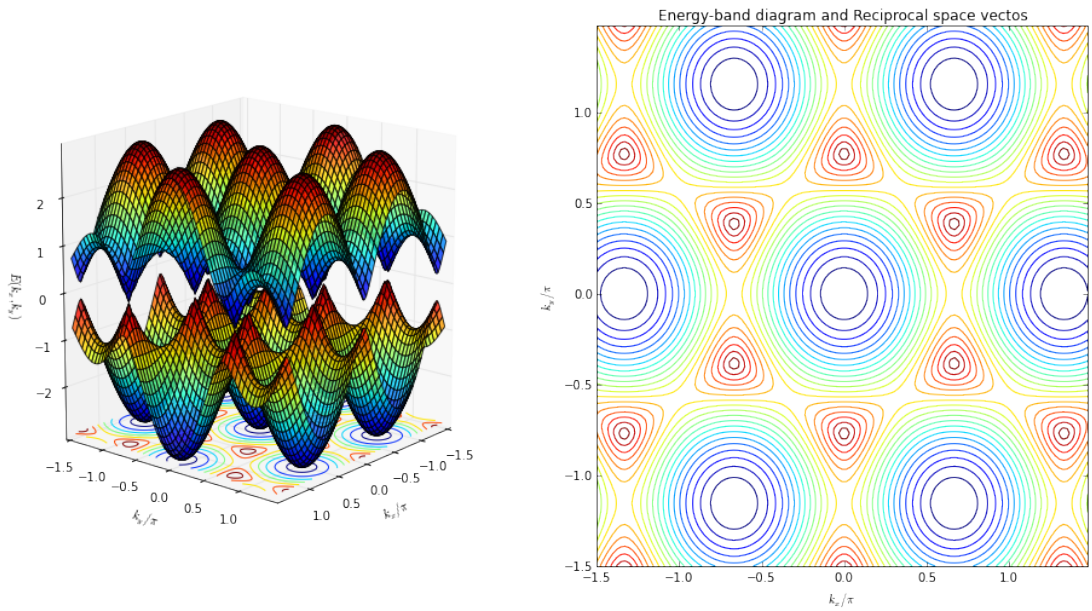

Figure 3.5: Energy-band diagram of honeycomb lattice. There are two-sites in a unit cell and two bands which do touch each other and form Dirac points.

Two equations are combined to give the following quadratic difference equation,

$$\begin{aligned}\epsilon^2\psi^A(m_1,m_2) &= t^2[3\psi^A(m_1,m_2)+\psi^A(m_1+1,m_2)+\psi^A(m_1,m_2+1)\\ &+ \psi^A(m_1-1,m_2)+\psi^A(m_1,m_2-1)+\psi^A(m_1-1,m_2+1)\\ &+ \psi^A(m_1+1,m_2-1)].\end{aligned}$$

The Hamiltonian and the translation operators along $\vec{a}_1$ and $\vec{a}_2$ commute, and therefore mutual eigenstates can be chosen as plane waves,

$$\psi_{k_1,k_2}(m_1,m_2) = ge^{ik_1m_1}e^{ik_2m_2}.$$

The energy dispersion relation is

$$\epsilon_{k_1,k_2} = \pm t\sqrt{3+2cos(k_1)+2cos(k_2)+2cos(k_1-k_2)}, \tag{3.8}$$

the corresponding energy-band diagram is in Fig.3.5.

In the presence of a magnetic field, the Hamiltonian is modified with Peierls

substitution and the Hamiltonian eigenvalue equation becomes

$$
\begin{aligned}
\hat{\mathcal{H}}|\Psi\rangle &= \epsilon|\Psi\rangle = -\sum_{m_1,m_2}\Big[\\
&+ \epsilon_0^A|m_1,m_2,A\rangle\langle m_1,m_2,A| \\
&+ \epsilon_0^B|m_1,m_2,B\rangle\langle m_1,m_2,B| \\
&+ t|m_1,m_2,A\rangle\langle m_1,m_2,B| \\
&+ t|m_1,m_2,B\rangle\langle m_1,m_2,A| \\
&+ t|m_1-1,m_2+1,A\rangle\langle m_1,m_2,B|e^{i\pi\Phi(m_2+1/2)} \\
&+ t|m_1+1,m_2-1,B\rangle\langle m_1,m_2,A|e^{-i\pi\Phi(m_2-1/2)} \\
&+ t|m_1,m_2+1,A\rangle\langle m_1,m_2,B|e^{-i\pi\Phi(m_2+1/2)} \\
&+ t|m_1,m_2-1,B\rangle\langle m_1,m_2,A|e^{i\pi\Phi(m_2-1/2)}\Big] \\
&\times \Big[\sum_{n_1,n_2}\psi^A(n_1,n_2)|n_1,n_2,A\rangle + \psi^B(n_1,n_2)|n_1,n_2,B\rangle\Big].
\end{aligned}
$$

The coupled difference equations are

$$
\begin{aligned}
&\left(\epsilon-\epsilon_0^B\right)\psi^B(m_1,m_2) = \\
&-t\Big[\psi^A(m_1,m_2)+e^{i\pi\Phi(m_2+1/2)}\psi^A(m_1,m_2+1)+e^{-i\pi\Phi(m_2-1/2)}\psi^A(m_1-1,m_2+1)\Big] \\
&\left(\epsilon-\epsilon_0^A\right)\psi^A(m_1,m_2) = \\
&-t\Big[\psi^B(m_1,m_2)+e^{-i\pi\Phi(m_2-1/2)}\psi^B(m_1,m_2-1)+e^{i\pi\Phi(m_2-1/2)}\psi^B(m_1+1,m_2-1)\Big].
\end{aligned}
$$

These two equations are periodic with a period of $2q$ when magnetic flux over flux quantum is written as a rational number $\phi = p/q$ where p, q are mutually prime numbers. Moreover, two coupled equations with $2q$ periodicity requires $4q$x$4q$ equations to be solved, but there are actually q independent equations[18].

We can reduce $4q$ equations into q independent equations through:

- put one difference equation into the other one eliminates ψ^A or ψ^B, we take $\epsilon_0^A = \epsilon_0^B = 0$ for simplicity,

- make a Gauge transformation and obtain periodicity of q.

The combined difference equation is as follows,

$$\begin{aligned}
&\epsilon^2\psi^A_{m_1,m_2} = \\
&t^2[\psi^A(m_1,m_2) + e^{+i\pi\Phi(m_2+1/2)}\psi^A(m_1,m_2+1) \\
+\ & e^{-i\pi\Phi(m_2+1/2)}\psi^A(m_1-1,m_2+1)] \\
+\ & t^2e^{-i\pi\Phi(m_2-1/2)}[\psi^A(m_1,m_2-1) + e^{+i\pi\Phi(m_2-1/2)}\psi^A(m_1,m_2) \\
+\ & e^{-i\pi\Phi(m_2-1/2)}\psi^A(m_1-1,m_2)] \\
+\ & t^2e^{+i\pi\Phi(m_2-1/2)}[\psi^A(m_1+1,m_2-1) + e^{+i\pi\Phi(m_2-1/2)}\psi^A(m_1+1,m_2) \\
+\ & e^{-i\pi\Phi(m_2-1/2)}\psi^A(m_1,m_2)].
\end{aligned}$$

A plane wave behaviour along $\vec{a}_1$ follows by the translational symmetry. Translation operator along y-direction commutes with the tight-binding Hamiltonian, and we can choose a plane wave solution as mutual eigenstates,

$$\psi_{m_1,m_2} = e^{ik_1m_1}g_{m_2}$$

The simplified equation is,

$$\begin{aligned}
(\epsilon^2-3)g_{m_2} &= t^2e^{ik_1/2}2cos(\pi\frac{p}{q}(m_2-1/2)-k_1/2)g_{m_2-1} \\
&+ t^2 2cos(2\pi\frac{p}{q}(m_2-1/2)-k_1)g_{m_2} \\
&+ t^2e^{-ik_1/2}2cos(\pi\frac{p}{q}(m_2+1/2)-k_1/2)g_{m_2+1}.
\end{aligned}$$

There are still $2q$ equations since the periodicity is $2q$. The following transformation[18] reduces to a set of q independent equations,

$$g_{m_2} = e^{i\pi\frac{p}{q}k_1m_2 - i\pi\frac{p}{q}m_2^2}f_{m_2}.$$

We define $\lambda \doteq (\epsilon^2-3)/t^2$, the final difference equation is

$$\begin{aligned}
\lambda f_{m_2} &= (1+e^{i2\pi\frac{p}{q}(m_2-1/2)-ik_1})f_{m_2-1} \\
&+ 2cos(2\pi\frac{p}{q}(m_2-1/2)-k_1)f_{m_2} \\
&+ (1+e^{-i2\pi\frac{p}{q}(m_2+1/2)+ik_1})f_{m_2+1},
\end{aligned}$$

where $k_1 = \vec{a}_1\cdot\vec{k} = a\sqrt{3}k_y$, $k_2 = \vec{a}_2\cdot\vec{k} = a\frac{3}{2}k_x + a\frac{\sqrt{3}}{2}k_y$.

Applying Bloch's theorem, we obtain $q\times q$ energy eigenvalue equation. The Hofstadter butterfly is shown in Fig.3.6.

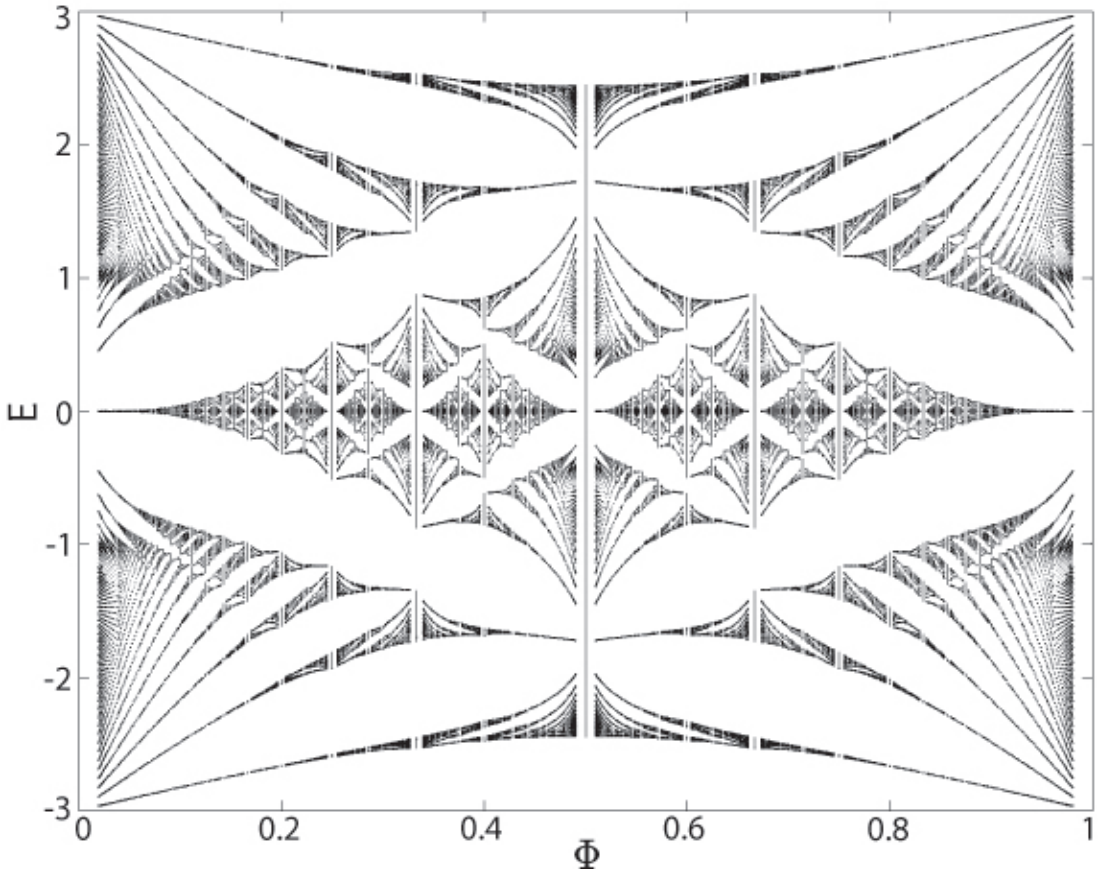

Figure 3.6: The Rammal-Hofstadter butterfly calculated for the honeycomb lattice up to $q = 51$

Chapter 4

Evolution of the Hofstadter Butterfly in a Tunable Optical Lattice Through Adiabatic Change of the Basis Vectors

The contents of this chapter ere partially expanded in the article published in Physical Review A Volume 91 in 23 June 2015 [20]

The Zurich research group realized an optical lattice system, where they can change the laser parameters and create different lattice geometries[3]. If the lattice parameters are changed, the evolution of the Hofstadter butterfly for different lattice geometries can be observed. In this chapter, we present the numerical solutions for all possible lattice parameters by the Zurich group, and calculate the corresponding Hofstadter butterflies.

The optical lattice system uses three lasers to create the checkerboard, the triangular, the dimer and the honeycomb like lattices by changing laser parameters. The potential corresponding to the artificial lattice is shown in Fig. 4.1. The

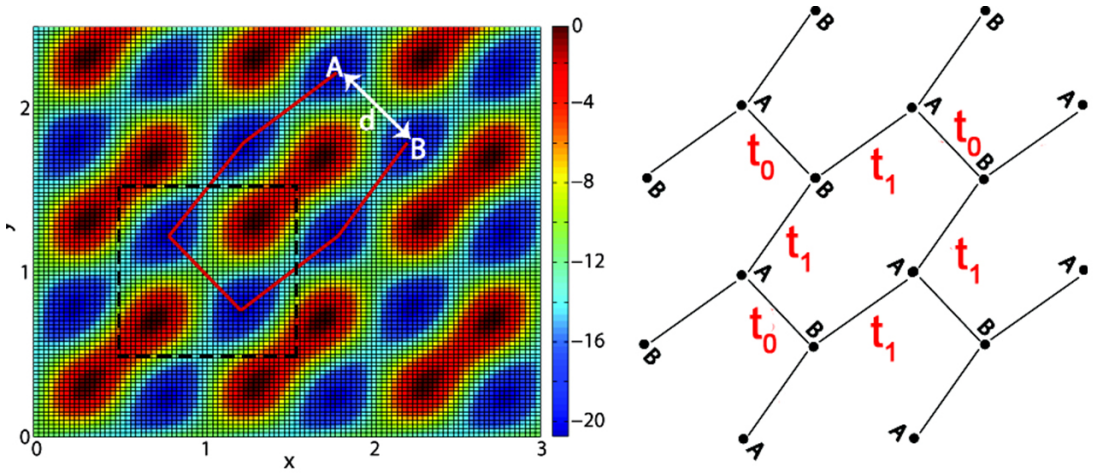

Figure 4.1: The real-space potential $V_{\bar{x}} = 14, V_x = 0.79, V_y = 6.45$ in units of recoil energy E_R and $\alpha = 0.9$. The square unit cell has two basis. This potential is used to demonstrate artificial graphene by Zurich group[12]. The tunneling amplitudes are obtained through projection of the two lowest band energies $t_0 = .., t_1 = ..$ that is calculated by numerical Schödinger equation. We rotate the lattice by $\pi/4$ so that the unit cell lies between $(0, 1)$ in x-y plane. The distance between two sites can be adjusted adiabatically so that the lattice geometry can evolve from the checkerboard to the honeycomb lattice. For this purpose, the potential parameters are changed and the distance d between the sites modifies the tunneling amplitudes.

potential is,

$$V(x,y) = V_{\bar{x}}\cos^2(kx+\theta/2)+V_x\cos^2(kx)+V_y\cos^2(ky)+2\alpha\sqrt{V_xV_y}\cos(kx)\cos(ky), \tag{4.1}$$

$V_{\bar{x}}, V_x, V_y$ are the potential depths, $k = 2\pi/\lambda$, λ is the wavelength of lasers. α is the visibility of the interference pattern, and the phases $\theta = \pi$ and $\varphi = 0$ are chosen to be the same as the experimental values.

The lattice is modeled by tight-binding Hamiltonian projected onto lowest two bands with nearest neighbor hoppings. The reason for lowest two bands is that there are two local minima in each unit cell and the number of energy bands is doubled. The derivation of the Hamiltonian starts from single particle continuous Schrödinger equation to the tight-binding model, which is discussed in Appendix A. The tunneling amplitudes for the model are fitted to the exact numerical energy eigenvalues of the Schrödinger Equation for each k_1 and k_2 couple. As

optical lattice parameters change, the Bravais lattice vectors do not change. This is an advantage for the calculations since the size of the unit cell does not change, and the general shape of the Brillouin zone is constant as well.

4.1 The Tight-Binding Hamiltonian without the Magnetic Field

We choose the primitive vectors for the optical lattice as,

$$\begin{aligned} \vec{a}_1 &= \hat{x} \\ \vec{a}_2 &= \hat{y}. \end{aligned}$$

They are made dimensionless with the lattice constant a and construct the Bravais vectors, $\vec{R}_{m_1,m_2} = m_1\vec{a}_1 + m_2\vec{a}_2$ where $(m_1, m_2) \in \mathbb{Z}$. The basis vectors are

$$\begin{aligned} \vec{d}_A &= \frac{d}{2\sqrt{2}}(-\hat{x} + \hat{y}) \\ \vec{d}_B &= \frac{d}{2\sqrt{2}}(\hat{x} - \hat{y}). \end{aligned}$$

It is a bipartite symmetric lattice where the band energies are symmetrical. Moreover, each site in a unit cell (site A) is going to be connected with the other site (site B). Every site has 3 nearest neighbours and nn tight binding model is,

$$\begin{aligned} \mathcal{H} &= -\sum_{m_1,m_2} \Big[\\ &+ \epsilon_0^A |m_1, m_2, A\rangle\langle m_1, m_2, A| \\ &+ \epsilon_0^B |m_1, m_2, B\rangle\langle m_1, m_2, B| \\ &+ t_0 |m_1, m_2, A\rangle\langle m_1, m_2, B| \\ &+ t_0 |m_1, m_2, B\rangle\langle m_1, m_2, A| \\ &+ t_1 |m_1 + 1, m_2, A\rangle\langle m_1, m_2, B| \\ &+ t_1 |m_1 - 1, m_2, B\rangle\langle m_1, m_2, A| \\ &+ t_1 |m_1, m_2 + 1, A\rangle\langle m_1, m_2, B| \\ &+ t_1 |m_1, m_2 - 1, B\rangle\langle m_1, m_2, A| \Big]. \end{aligned}$$

We seek eigenstates $\mathcal{H}|\Psi\rangle = \epsilon|\Psi\rangle$ for the Hamiltonian, and the real space expansion is as follows:

$$|\Psi\rangle = \sum_{n_1,n_2} \psi^A(n_1,n_2)|n_1,n_2,A\rangle + \psi^B(n_1,n_2)|n_1,n_2,B\rangle.$$

A coupled difference equation is obtained for the eigenvalue equation:

$$-t_0\psi^A(n_1,n_2) - t_1\psi^A(n_1+1,n_2) - t_1\psi^A(n_1,n_2+1) = \left(\epsilon - \epsilon_0^B\right)\psi^B(n_1,n_2)$$

$$-t_0\psi^B(n_1,n_2) - t_1\psi^B(n_1-1,n_2) - t_1\psi^B(n_1,n_2-1) = \left(\epsilon - \epsilon_0^A\right)\psi^A(n_1,n_2)$$

We eliminate the self-energy terms and combine the equations. Assuming plane wave behavior along $\vec{a_1}$ and $\vec{a_2}$ and $\psi^{A,B}(n_1,n_2) = ge^{ik_1n1}e^{ik_2n_2}$, we get

$$\begin{aligned}
\epsilon^2 ge^{ik_1n_1}e^{ik_2n_2} &= [(t_0^2+2t_1^2)ge^{ik_1n_1}e^{ik_2n_2} \\
&+ t_0t_1ge^{i(k_1+1)n_1}e^{ik_2n_2} + t_0t_1ge^{ik_1n_1}e^{ik_2(n_2+1)} \\
&+ t_0t_1ge^{ik_1(n_1-1)}e^{ik_2n_2} + t_1^2ge^{ik_1(n_1-1)}e^{ik_2(n_2+1)} \\
&+ t_0t_1ge^{ik_1n_1}e^{ik_2(n_2-1)} + t_1^2ge^{ik_1(n_1+1)}e^{ik_2(n_2-1)}].
\end{aligned}$$

The diagonalization of the Hamiltonian is done through Fourier transformation,

$$\epsilon_{k_1k_2} = \pm\sqrt{t_0^2 + 2t_1^2 + 2t_0t_1\cos(k_1) + 2t_0t_1\cos(k_2) + 2t_1^2\cos(k_1-k_2)}, \qquad (4.2)$$

where $k_1 = \vec{k}\cdot\vec{a_1} = k_x$, $k_2 = \vec{k}\cdot\vec{a_2} = k_y$.

Before continuing our calculations with finite magnetic field, we need to explain how the optical lattice system is modeled with the nn tight-binding model ensuring the reliability of our analysis throughout the calculations. For this purpose, the tunneling amplitudes of tight-binding Hamiltonian are estimated from each set of optical lattice parameter. This procedure starts with the numerical solution to the potential generated with optical tunable lattice. The energy eigenvalues for the lowest two bands are obtained. Therefore, it is going to be compared to the tight-binding energy dispersion relation over the whole Brillouin zone. Consequently, it becomes possible to use LMSE (Least mean-square error) method to fit t_0 and t_1.

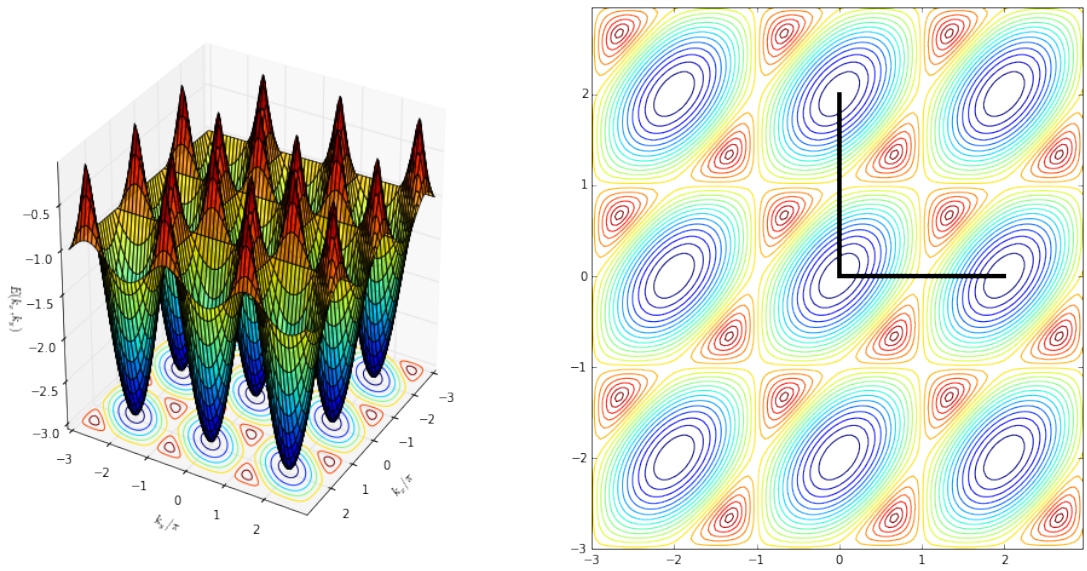

Figure 4.2: The energy-band diagram of the honeycomb lattice. The Brillouin zone is square since the real-space unit cell is square. Each site has three nearest neighbors as in the honeycomb lattice.

4.2 The Tight-Binding Hamiltonian under a Magnetic Field

In order to obtain the tight-binding Hamiltonian under finite magnetic field, we need to include the hopping phases that each projection operator gains during hopping. The hopping phase is dependent on the line integral of the Landau gauge along the path. This integral is evaluated as,

$$\Theta_{mn}^{ij} = \frac{q}{\hbar c}\int_{\vec{R}_{m,i}}^{\vec{R}_{n,j}} \vec{A}\cdot d\vec{\ell} = 2\pi\Phi\left(\hat{y}\cdot(\vec{R}_n - \vec{R}_m + \vec{d}_j - \vec{d}_i)\right)\left[\hat{x}\cdot\frac{\vec{R}_n+\vec{R}_m+\vec{d}_j+\vec{d}_i)}{2}\right],$$

$\Phi = \phi/\phi_0$, where $\phi_0 = hc/e$ and $\phi = Ba^2$ in the checkerboard lattice. The hopping phase then evaluated as,

$$\Theta_{mn}^{ij} = 2\pi\Phi\left(s_1 + \frac{\hat{y}\cdot(\vec{d}_j-\vec{d}_i)}{a}\right)\left[m_2 + \frac{s_2}{2} + \frac{\hat{x}\cdot(\vec{d}_j+\vec{d}_i)}{2a}\right]$$

where $(s_1, s_2) = (n_1 - m_1, n_2 - m_2)$ and i, j corresponds to sites A, B.

Hence the Hamiltonian becomes

$$\begin{aligned}\mathcal{H} = -\sum_{m_1,m_2} \Big\{ & t_0 |m_1, m_2, A\rangle\langle m_1, m_2, B| e^{-i2\pi\Phi d' m_1} \\ & + t_1 |m_1+1, m_2, A\rangle\langle m_1, m_2, B| e^{-i2\pi\Phi d'(m_1+\frac{1}{2})} \\ & + t_1 |m_1, m_2-1, A\rangle\langle m_1, m_2, B| e^{-i2\pi\Phi(d'-1)m_1} + h.c. \Big\}, \end{aligned} \tag{4.3}$$

and d' is defined as $\frac{d}{\sqrt{2}}$, $h.c$ stands for the Hermitian conjugate.

The phase gained circulating around a unit cell is $[0,0,B \to 0,1,A](\Delta\phi = 2\pi\Phi d'\frac{1}{2})[0,1,A \to 0,1,B](\Delta\phi = -2\pi\Phi d')[0,1,B \to 1,1,A](\Delta\phi = 2\pi\Phi(d'-1))[1,1,A \to 1,0,B](\Delta\phi = -2\pi\Phi d'\frac{1}{2})[1,0,B \to 1,0,A](\Delta\phi = 0)[1,0,A \to 0,0,B](\Delta\phi = 0)$, in total $-2\pi\Phi$ as it should be. The magnetic unit cell is enlarged q times for a rational magnetic flux value, $\Phi = p/q$, ensuring magnetic translation invariance.

We seek eigenstates $\mathcal{H}|\Psi\rangle = \epsilon|\Psi\rangle$ and ϵ is the energy eigenvalue,

$$|\Psi\rangle = \sum_{n_1,n_2} \psi^A(n_1,n_2)|n_1,n_2,A\rangle + \psi^B(n_1,n_2)|n_1,n_2,B\rangle.$$

Two coupled difference equations are obtained from the eigenvalue equation:

$$\begin{aligned}\epsilon\psi^B_{m_1,m_2} = & -t_1 e^{i2\pi\Phi d'(m_1+1/2)}\psi^A_{m_1+1,m_2} \\ & - t_0 e^{i2\pi\Phi d' m_1}\psi^A_{m_1,m_2} \\ & - t_1 e^{-i2\pi\Phi(1-d')m_1}\psi^A_{m_1,m_2-1}, \end{aligned} \tag{4.4}$$

$$\begin{aligned}\epsilon\psi^A_{m_1,m_2} = & -t_1 e^{-i2\pi\Phi d'(m_1-1/2)}\psi^B_{m_1-1,m_2} \\ & - t_0 e^{-i2\pi\Phi d' m_1}\psi^B_{m_1,m_2} \\ & - t_1 e^{i2\pi\Phi(1-d')m_1}\psi^B_{m_1,m_2+1}, \end{aligned} \tag{4.5}$$

Substituting one of the equations into another, we get a finite difference equation,

$$\begin{aligned}\epsilon^2\psi^A_{m_1,m_2} &= (t_0^2+2t_1^2)\psi^A_{m_1,m_2}\\ &+ t_0t_1\Big\{e^{i2\pi\Phi m_1}\psi^A_{m_1,m_2-1}+e^{-i\pi\Phi d'}\psi^A_{m_1-1,m_2}\\ &+ e^{i2\pi\Phi m_1}\psi^A_{m_1,m_2+1}+e^{i\pi\Phi d'}\psi^A_{m_1+1,m_2}\Big\}\\ &+ t_1^2\Big\{e^{-i2\pi\Phi(m_1-1)}e^{-i\pi\Phi d'}\psi^A_{m_1-1,m_2-1}\\ &+ e^{i2\pi\Phi m_1}e^{i\pi\Phi d'}\psi^A_{m_1+1,m_2+1}\Big\}. \end{aligned} \tag{4.6}$$

The translation operator along $\vec{a_2}$, $\hat{T}(\hat{a}_2\cdot\vec{x})$ and Hamiltonian are commuting operators, $\left[\hat{T}(\hat{a}_2\cdot\vec{x}),\hat{\mathcal{H}}\right]=0$. Therefore, we can seek mutual eigenstates for both operators. In other words, the Hamiltonian (hence the difference equation) does not depend on n_1. Thus the solutions can be chosen as

$$\psi_{m_1,m_2}(k_y) = e^{ik_ym_2}e^{-i\pi\Phi d'm_1}f_{m_1},, \tag{4.7}$$

where k_y is quasi momentum along the y-direction. Reorganizing the terms in a simplified manner, we obtain the following one-dimensional difference equation,

$$\begin{aligned}\lambda f_{m_1} &= \left(1+\frac{t_1}{t_0}e^{-i(2\pi\Phi(m_1-1)+k_y)}\right)f_{m_1-1}\\ &+ 2\cos(2\pi\Phi m_1+k_y)f_{m_1}\\ &+ \left(1+\frac{t_1}{t_0}e^{i(2\pi\Phi m_1+k_y)}\right)f_{m_1+1}. \end{aligned} \tag{4.8}$$

The eigenvalues are defined as

$$\lambda = \frac{\epsilon^2-(t_0^2+2t_1^2)}{t_0t_1}. \tag{4.9}$$

If we assume Φ to be a rational number, $\Phi=\frac{p}{q}$, with p,q mutually prime integers, the equation is symmetric under translation by q indices. This is a good place to discuss the shape of the magnetic unit cell, and the restrictions on it.

$$-\frac{\pi}{q}\le k_x<\frac{\pi}{q},\ -\pi\le k_y<\pi.$$

In the presence of a finite uniform magnetic field, $\Phi=p/q$, the magnetic unit cell is expanded in real space along $\vec{a}_2$ by q. In the reciprocal space, only $\vec{b}_2$ contracts by q.

Applying the Bloch theorem, the system is reduced into a set of q independent difference equations,

$$\begin{aligned}
\lambda_{k_y} f_0 &= \left(1 + t_{10} e^{-i(2\pi\Phi(-1)+k_y)}\right) f_{-1} \\
&+ 2\cos(2\pi\Phi 0 + k_y) f_0 + \left(1 + t_{10} e^{i(2\pi\Phi 0+k_y)}\right) f_1 \\
\lambda_{k_y} f_1 &= \left(1 + t_{10} e^{-i(2\pi\Phi(0)+k_y)}\right) f_0 \\
&+ 2\cos(2\pi\Phi 1 + k_y) f_1 + \left(1 + t_{10} e^{i(2\pi\Phi 1+k_y)}\right) f_2 \\
&\ldots \\
\lambda_{k_y} f_{q-1} &= \left(1 + t_{10} e^{-i(2\pi\Phi(q-2)+k_y)}\right) f_{q-2} \\
&+ 2\cos(2\pi\Phi(q-1) + k_y) f_{q-1} + \left(1 + t_{10} e^{i(2\pi\Phi(q-1)+k_y)}\right) f_q. \quad (4.10)
\end{aligned}$$

Then, the Bloch theorem allows us to write

$$f_{n+q} = e^{iqk_x} f_n.$$

The effect of the magnetic field on the system is easy to visualize when the energy-band diagram is plotted for a particular $\Phi = \frac{p}{q}$ values. We first plot the bands for $\Phi = 1/3$ and determine the maximum and minimum points for each band. As seen in the energy band diagram for $\phi = 1/3$, the Brillouin zone is 3-fold degenerate as a consequence of Floquet's theorem. Therefore it is possible to use the reduced unit cell without any information loss.

4.3 Determining the Critical Points of the Energy Bands

A set of q independent difference equations forms a $q \times q$ energy eigenvalue matrix equation for particular k_x, k_y values, $W(k_x, k_y)\underline{f} = \underline{\lambda f}$. The secular determinant of $W(k_,k_y)$ is set to zero for non-trivial energy eigenvalues.

It is time to analyse the determinant in detail and obtain the maximum and minimum values of energy for all $\vec{k}$ values so that we reduce the computational work. The difference equation does not change itself as $m_1 \to m_1 + q$.

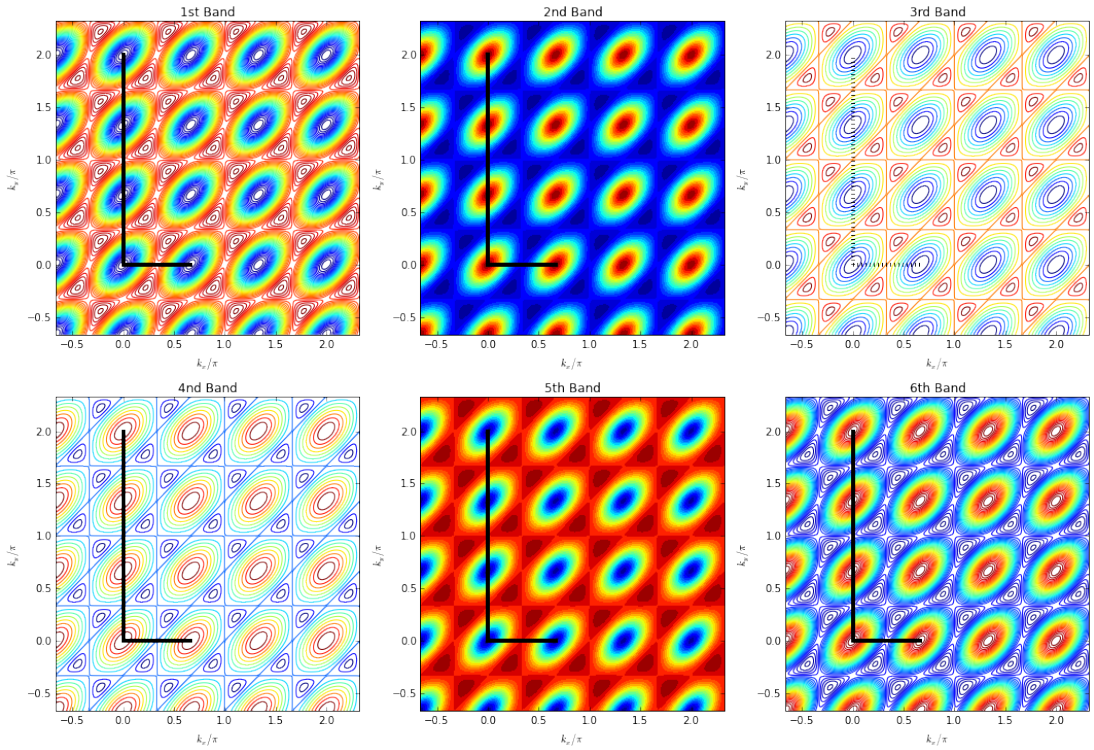

Figure 4.3: Energy-band diagram of modeled optical lattice for $\Phi = 1/3$, $t_0 = t_1 = 1$. The periodicity becomes $q = 3$ along $\vec{a}_1$ direction or m_1 index, which means the Brillouin zone shrinks by factor of 3 along $\vec{b_1}$. Moreover, Brillouin zone splits into $q = 3$ degenerate parts along $\vec{b_2}$.

Table 4.1: Critical (k_x, k_y) Momentum Pair for the Minimum and Maximum Values of the Energy Bands at $\Phi = p/q$.

	$\left(\frac{t_1}{t_0}\right)^q > \frac{1}{2}$	$\left(\frac{t_1}{t_0}\right)^q < \frac{1}{2}$
q even	$(qk_x, qk_y) = \left(\mp\cos^{-1}\frac{1}{2}\left(\frac{t_1}{t_0}\right)^{-q}, \pm\cos^{-1}\frac{1}{2}\left(\frac{t_1}{t_0}\right)^{-q}\right)$ $(qk_x, qk_y) = (\pi, \pi)$	$(k_x, k_y) = (0, 0)$ $(qk_x, qk_y) = (\pi, \pi)$
q odd	$(qk_x, qk_y) = \left(\pi \mp\cos^{-1}\frac{1}{2}\left(\frac{t_1}{t_0}\right)^{-q}, \pi \pm\cos^{-1}\frac{1}{2}\left(\frac{t_1}{t_0}\right)^{-q}\right)$ $(k_x, k_y) = (0, 0)$	$(qk_x, qk_y) = (\pi, \pi)$ $(k_x, k_y) = (0, 0)$

The secular determinant is defined as $D(\lambda, k_x, k_y) \doteq det(W(k_x, k_y) - \lambda I) = 0$. It is a q^{th} order polynomial of λ.

$D(\lambda, k_x, k_y)$ satisfies

$$D(\lambda, k_x, k_y) = D(\lambda, k_x, k_y + 2\pi/q) = D(\lambda, k_x + 2\pi/q, k_y). \tag{4.11}$$

The periodicity in k_y is due to q site periodicity in real space, the magnetic unit cell. In addition, the periodicity in k_x is due to the q-fold degeneracy along the k_x direction by the Floquet's theorem.

The terms in the secular equation which are independent of λ can be calculated as,

$$\begin{aligned}\mathbb{D}(k_x, k_y) = (-1)^{q+1}\cos(qk_x) + (-1)^{p(q-1)}\cos(qk_y) \\ + (-1)^{p(q-1)+q+1}\left(\frac{t_1}{t_0}\right)^q \cos(q(k_x + k_y)).\end{aligned} \tag{4.12}$$

These special $\vec{k}$ points are given in Table.4.1.

The estimation of the tunneling amplitudes for specific optical lattice parameters and the calculation of the Hofstadter butterfly for those tunneling rates are numerically efficient. The next section distinguishes and investigates three different energy spectra and discusses the transitions between them.

Chapter 5

The Energy Spectra and the First Chern Number for the Optical Lattice Parameters

The content of this chapter were partially published in Physical Review A Volume 91 in 23 June 2015 [20]

In the previous section, we explained how to calculate the Hofstadter butterflies for all experimental lattice parameters in Ref.[3]. Now, we analyse the results. What is called Hofstadter butterfly is Lebesgue zero measure fractal spectrum consisting of infinitely self-repeating energy gaps[21]. The closure of any two gaps result in a topologically different spectrum and physical properties as well. The smaller the gaps in the spectrum are, the less likely it is to observe them experimentally because of the temperature effects, imperfections, finite size effects [22] or edge states. The closing of the largest gaps in the spectrum are easiest to observe.

5.1 The Energy Spectra of the Adiabatic Lattice Transition from the Checkerboard Lattice to the Honeycomb Lattice

The butterfly energy spectrum can be divided into three categories as the major gaps are examined. The first category is the energy spectra consisting of two square lattice Hofstadter butterflies separated by an energy gap. The next category is similar to the honeycomb lattice Hofstadter butterfly except for the presence of infinite number of small gaps. The third category is the honeycomb lattice butterfly (the Hofstadter-Rammal butterfly).

The transition, starting from the first category till the third energy spectra, is non-trivial. The spectrum is plotted for the rational values of the magnetic flux per unit cell, $\Phi = p/q$, and the major gaps near zero energy do not close simultaneously as the lattice geometry transforms from the square to the honeycomb-like structure. The critical lattice parameter is distinct for each q value. As the central zero energy gap is closed for a specific $\Phi = p/q$ value, this gap fractures into smaller and self-similar gaps. We choose four different sets of lattice parameters where the resulting energy spectra are topologically distinct[23].

In the experiment, the geometry is tuned by organizing the potential inside a unit cell keeping the shape of the unit cell constant. Specifically, the Bravais lattice remains square. By adjusting the number, the deepness and the position of the potential minima, it is possible to obtain square, dimer and honeycomb like lattices. If we understand the periodic potential a in real-space unit cell, different energy spectra can be interpreted as well. The parameter θ in Eq.4.1 determines if the potential has one or two minima in a unit cell if the other parameters are kept constant. This transition can be modeled with a tight-binding Hamiltonian with three nearest neighbors if the neighboring Wannier functions which are accumulated around potential minima have small overlaps. Then, it is possible to project the system into tight-binding Hamiltonian with the lowest two energy states. The two bands obtained from these two states forms the

fractal energy band spectra with a gap in between. This gap can be controlled by the amount of overlap between the Wannier functions. The lattice in the dimer and checkerboard regimes, the energy spectrum in the presence of the magnetic field is made of two square lattice Hofstadter butterflies.

Our first example is the spectrum obtained for the experimental parameters $V_{\bar{x}} = 4.5, V_x = 1, V_y = 5$ and $\alpha = 0.95$. For these parameters, each real space unit cell has two local minima which are close to each other compared to the distance to the neighboring unit cells. This lattice is called dimer lattice(see Fig.5.1). We calculated the estimated values for tunneling amplitudes for the given lattice parameters as $t_0 = 0.3488$, $t_1 = 0.0843$. The corresponding Hofstadter butterfly is plotted in Fig.5.1. The energy spectrum consists of two square lattice butterflies separated by a large energy gap. It can be observed that the centers of square butterflies are controlled by t_0, in-cell hopping parameter while the width of the square butterflies are controlled by t_1. The lower band is generated by square lattice bonding states and the upper band by anti-bonding states in each unit cell. As the distance between potential minima in a unit cell increases, the in-cell tunneling amplitude, t_0, decreases. Simultaneously, the distance between adjacent cells decreases and the overlap of inter-cell Wannier functions increase t_1. This process makes the system closer to honeycomb regime. When there is no magnetic field, the band structure shows the creation of Dirac points at the zone corners. The first topological transition happens and the gaps at $\Phi = 0, 1$ are closed. Dirac point appears as long as $\frac{t_1}{t_0} \leq \frac{1}{2}$. This critical value was used to distinguish the honeycomb regime in the previous experimental and theoretical work[3, 24].

In the presence of a non-zero magnetic field, the lattices which have Dirac points at zero field do not guarantee the existence of Dirac points or closed gaps. In Fig.5.2, the butterfly is illustrated for the lattice parameters $V_{\bar{x}} = 12, V_x = 0.79, V_y = 6.45$ and $\alpha = 0.9$. This spectrum is significant because there are two square Hofstadter butterflies touching and forming Dirac points only at the edges. However, the gap between the butterflies remains for all rational flux values. In the light of the shape of the spectrum under the magnetic field, it is convenient to state that the spectrum is closer to two square Hofstadter butterflies on top

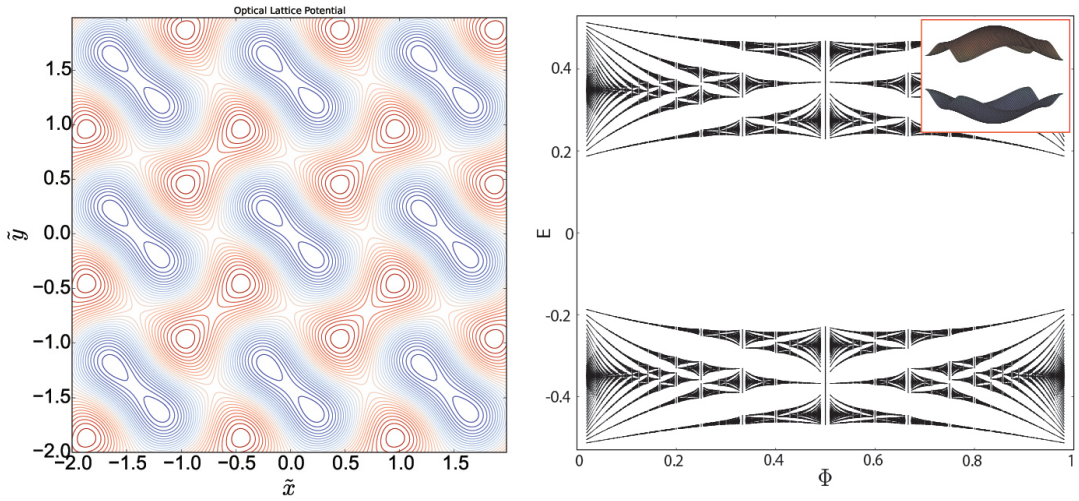

Figure 5.1: Real-space lattice potential and the corresponding energy spectrum as a function of magnetic flux per unit cell. For $V_{\bar{x}} = 4.5, V_x = 1, V_y = 5$ and $\alpha = 0.95$, we have lattice in a Dimer regime. The energies are normalized with the recoil energy, E_R, and flux is normalized with the flux quantum. Estimated tunneling amplitudes are $t_0 = 0.3488$ and $t_1 = 0.0843$ in E_R. The fractal spectrum is made of two square lattice Hofstadter butterflies separated by a large gap. The center of the butterflies are at t_0 while the widths are proportional to t_1. Inset shows the energy bands at zero field as a function of k_x, k_y. The largest gap at zero field is maintained at non-zero field, as well.

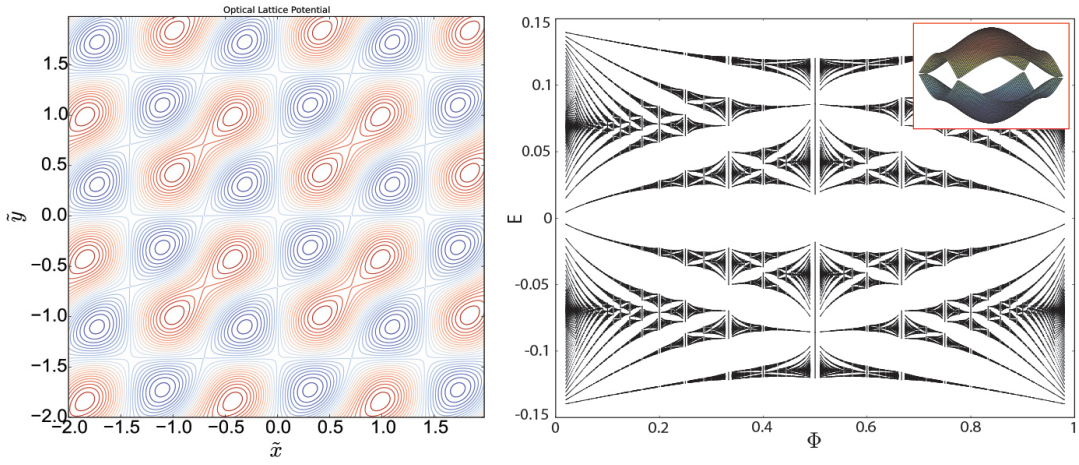

Figure 5.2: Real-space lattice potential and the corresponding energy spectrum as a function of magnetic flux per unit cell. For $V_{\bar{x}} = 12, V_x = 0.79, V_y = 6.45$ and $\alpha = 0.9$, the spectrum is barely at the honeycomb topological regime. Estimated tunneling amplitudes are $t_0 = 0.0691$ and $t_1 = 0.0361$ in E_R. Comparing with Fig.4.3, two square lattice Hofstadter butterflies comes near and touch only at $\Phi = 0, 1$. In addition, the inset shows the emergence Dirac points at zero field. In the presence of finite field, however, there occurs a energy gap at zero energy.

of each other. Now, we analyse a lattice closer to the honeycomb lattice. The tunneling amplitudes are $t_0 = 0.0441, t_1 = 0.0361$ and these hopping values can be generated by $V_{\bar{x}} = 13.5, V_x = 0.79, V_y = 6.45$ and $\alpha = 0.9$. The central gap splits into four big parts. The gap closings are only at flux $p/q = 0, 1/3, 1/2, 2/3, 1$.

We find an analytical formula of the critical ratio $t^c_{1,0} = t_1/t_0$ for the closing of a gap at a particular flux. Dirac point admits a zero point energy solution for the coupled equations Eq.4.5 and Eq.4.4. When the self energy terms are omitted and the energy is set to zero, the difference equations are uncoupled and solved with q fold iteration equivalence up to a Bloch phase,

$$\left(\frac{t_1}{t_0}\right)^{-q} + (-1)^{p(q-1)} e^{ik_x q} = (-1)^q e^{ik_y q}. \tag{5.1}$$

This equation has solution for some point in the Brillouin zone only if

$$\frac{t_1}{t_0} \geq \frac{1}{2^{1/q}}. \tag{5.2}$$

For a mutually prime rational flux value $\Phi = \frac{p}{q}$, zero energy gap is ensured to be close if $\frac{t_1}{t_0} \geq \frac{1}{2^{1/q}}$. The critical value is independent of the integer value of p. The

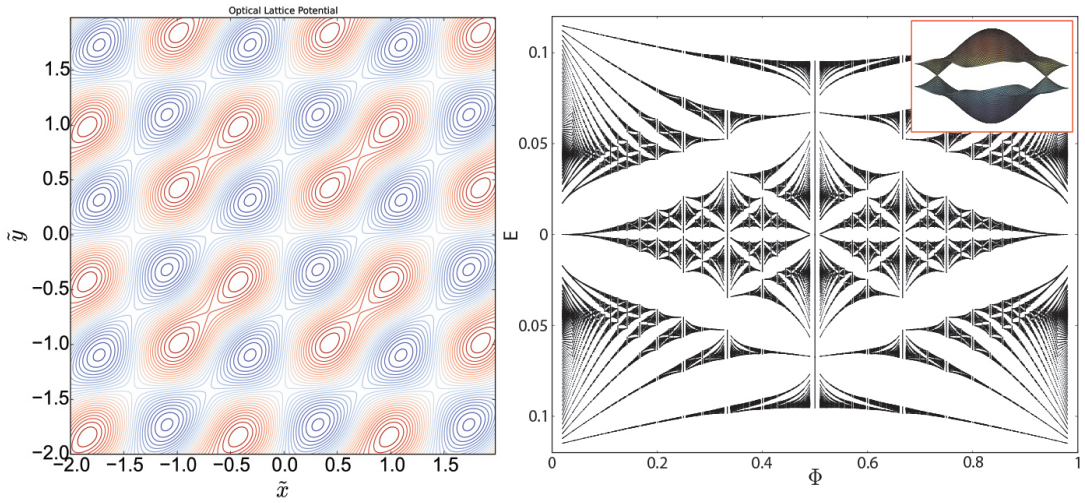

Figure 5.3: Real-space lattice potential and the corresponding energy spectrum as a function of magnetic flux per unit cell. For $V_{\bar{x}} = 13.5, V_x = 0.79, V_y = 6.45$ and $\alpha = 0.9$, the spectrum is in the deeper honeycomb topological regime. Estimated tunneling amplitudes are $t_0 = 0.0441$ and $t_1 = 0.0361$ in E_R. The Dirac points emerge at the edges ($\Phi = 0, 1$) and the flux values $p/q = 1/2, 1/3, 2/3$. The parameter $\frac{t_1}{t_0} = 0.0819$, Eq.5.2 shows that the bands around zero energy do not touch at all rational flux values with $q > 3$. The main gap at zero energy is fractured into four parts. The inset is topologically same with the inset in Fig.5.2, except the position of Dirac points. This indicates that it is not possible to determine the energy spectra for finite magnetic field through analysing only the non-zero field case.

evolution of the energy spectrum from the dimer to the honeycomb lattice, the first closing of the bands is for zero field where the periodicity of the unit cell is $q = 1$. Therefore the critical value is at $t^c_{1,0} = \frac{1}{2^{1/1}} = \frac{1}{2}$. For the ratio between $0.5 < \frac{t_1}{t_0} < \frac{1}{\sqrt{2}} \simeq 0.7071$, there is no gap closing and no zero energy solution in the presence of magnetic field. Following the gap closing at flux $\Phi = 1/2$, the next flux values to have gap closings are $\Phi = \frac{1}{3}, \frac{2}{3}$ at $\frac{t_1}{t_0} = \frac{1}{2^{1/3}} \simeq 0.7937$. The spectrum is plotted in Fig.5.3 for $\frac{t_1}{t_0} = 0.819$. The central gap is fractured into four parts.

The merging of two square lattice Hofstadter butterflies to form a honeycomb butterfly is a topologically non-trivial process. As discussed in Eq.5.2, there must be an infinite number of sequential gap closings. The critical values for the gap closings at zero energy depend only on the denominator of a particular flux, q in a simple but non-analytic way. The closings of the gaps finalises when $t^c_{1,0} = 1$, and this actually corresponds to the honeycomb lattice.

We must determine if the optical parameters that were used to demonstrate graphene structure [12] maintain the same characteristics at finite magnetic field. We calculated the Hofstadter energy spectra for the experimental parameters that were used to realize artificial graphene, as seen in Fig.5.4. The estimated tunneling amplitudes give the ratio $t^c_{1,0} = 0.923$, which tells us that the central energy gap is closed for all flux values, $\Phi = p/q$ where $q < 9$. Although the central gaps are not fully closed as in ideal graphene (see Fig.3.6), the general shape of the energy spectra is almost the same apart from small unclosed gaps. The outcomes of the energy spectral analysis can be candidate for the realization of graphene until the energy resolution of measurement systems are finer than a typical size of the energy gaps.

We described the characteristics of the spectrum that can be obtained by the optical lattice parameters within the current experimental capabilities. In the next section, we calculate the first Chern numbers of the gaps and discuss the evolution of the topological properties.

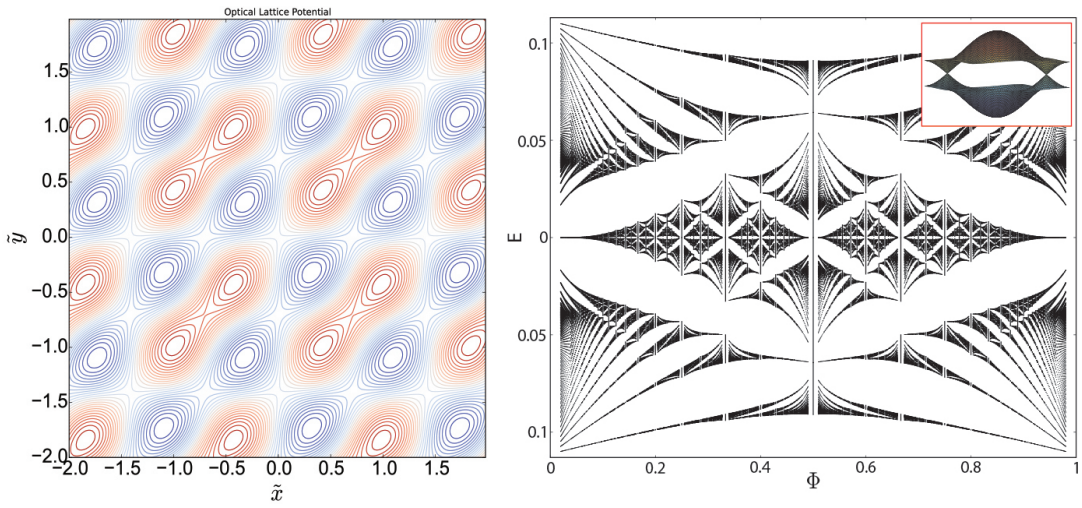

Figure 5.4: Real-space lattice potential and the corresponding energy spectrum as a function of magnetic flux per unit cell. The parameters $V_{\bar{x}} = 14, V_x = 0.79, V_y = 6.45$ and $\alpha = 0.9$, are utilized to demonstrate graphene [12]. Estimated tunneling amplitudes are $t_0 = 0.0391$ and $t_1 = 0.0361$ in E_R. For these values, the energy spectra almost overlaps with graphene Hofstadter butterfly as seen in Fig.3.6. The only difference is the open gaps for $\Phi = p/q$ values whose denominator is $q \geq 9$ around zero energy. The inset shows the translation of Dirac points.

5.2 The First Chern Number and Topological Properties of the Adiabatic Tunable Lattice Transition

Each Bloch energy band (and gap) in the presence of magnetic field is associated with an integer which is a topological invariant. This invariant is called the first Chern number and the contribution of each band to the Hall conductance turns out to be e^2/h times this integer[25]. The perturbative effects in the lattice potential or the magnetic field does not affect the Chern number for particular energy band. It allows associating each gap with a particular Chern number as well[26]. Moreover, the Hall conductivity is proportional to Chern number, $\sigma_{xy} = \nu e^2/h$ as long as the Fermi energy is confined within a energy gap with Chern number ν. The conductivity is a measurable operator and lets theoreticians and experimentalists investigate the topological and physical properties of a specific system[27, 28, 29, 30, 31]. There are several novel measurement methods for

cold atom systems to detect the Chern number and the Berry curvature. From a historical point of view, the calculation or measurement of the Chern number was used to require a long procedure, but the Středa formula greatly simplifies both the experimental and numerical measurement of the Chern number [32]. This formula approaches the problem from a statistical perspective and defines the Hall conductivity as the differential change of the density of states with changes in magnetic flux. The conductivity is

$$\sigma_{xy} = \frac{\partial N}{\partial B},$$

N represents the number of states below the Fermi energy which is defined in a band gap. Since the cold atom experiment setups are more favorable to measure density instead of transport properties of a system, we can comfortably utilize this relation [22]. The relation, for a cold atom system, can be modified when each term is multiplied with the area of the unit cell:

$$\nu = \frac{\partial n}{\partial \Phi}, \tag{5.3}$$

n is the density of fermions in each unit cell and $\Phi = \phi/\phi_0$ is the magnetic flux per unit cell normalized by the flux quantum.

The numerical calculation of Chern numbers for each energy gap turn into the counting of the number of bands below the Fermi energy with the Eq.4.10 for two closely spaced flux values and obtaining the derivative as a difference[22]. We investigate the evolution of the bands from the checkerboard to the honeycomb structure for particular flux values. Starting with $\Phi = 1/3$, all the large gaps except the central gap remains open throughout the evolution as shown in Fig.5.5. The gaps with Chern numbers ± 1 are preserved for $0 < \frac{t_1}{t_0} \leq 1$. The lower limit indicates two separate square lattice bands and the upper limit indicates the honeycomb lattice bands. Two bands around zero energy merge at $\frac{t_1}{t_0} = \frac{1}{2^{1/3}}$ and the main gap with zero Chern number diminishes and disappears.

As we discussed in Sec.5.1, the central gap fractures into smaller gaps and disappears when $\frac{t_1}{t_0} = 1$. However, the progress is not trivial for other gaps. the closing and reopening of infinitely many gaps during the transition can be observed in [23]. What we know about this transition is quite limited. The total number

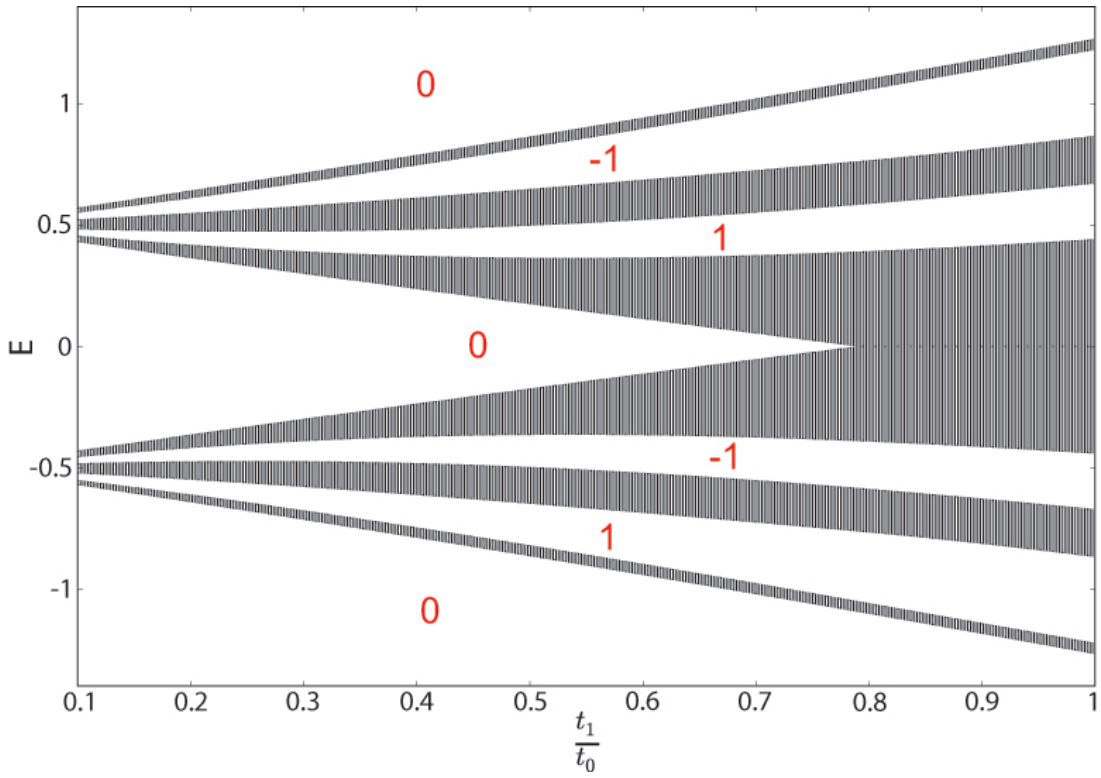

Figure 5.5: The evolution of bands for flux $\Phi = 1/3$ from the checkerboard to the honeycomb regime as a function of $\frac{t_1}{t_0}$. We labeled the gaps with their Chern number. Only the gap with zero Chern number is closed throughout the transition. The main gap is closed at $\frac{t_1}{t_0} = \frac{1}{2^{1/3}}$. In the lower limit of $\frac{t_1}{t_0}$, the energy gap between mirror symmetric bands with respect to zero energy resembles the two square lattice butterflies. In the upper limit where the ratio approaches one, the spectra gets closer to honeycomb lattice butterfly.

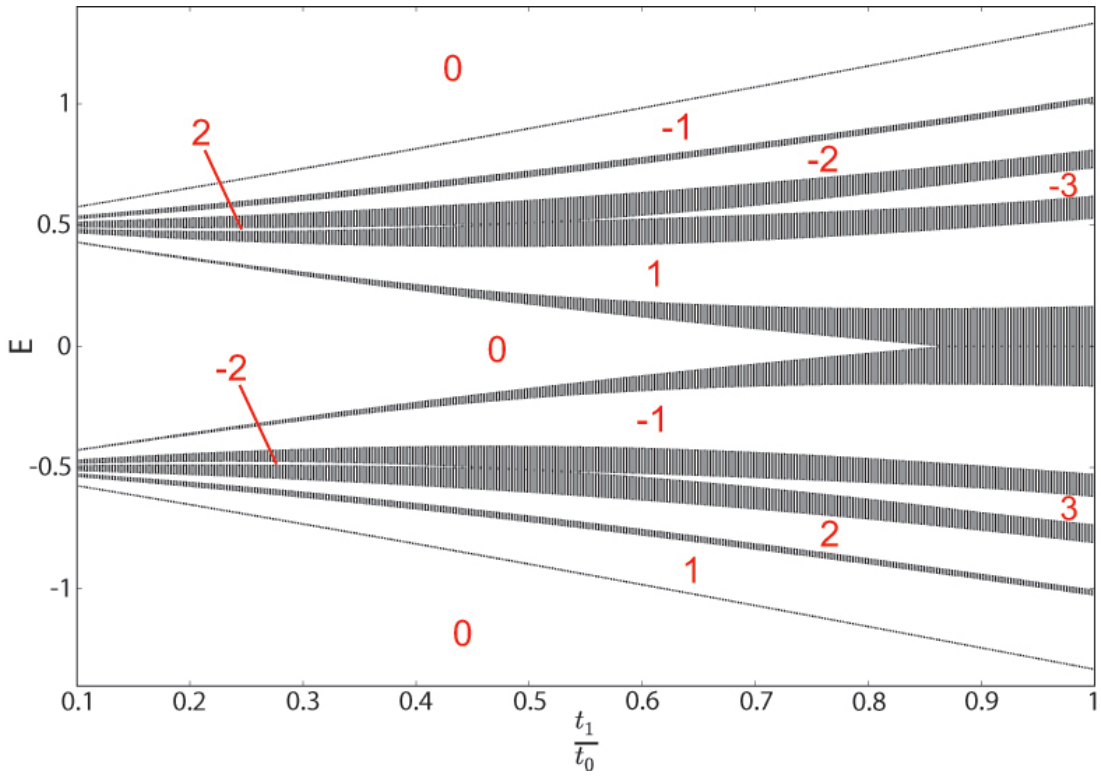

Figure 5.6: The evolution of bands for flux $\Phi = 1/5$ from the checkerboard to the honeycomb regime as a function of $\frac{t_1}{t_0}$. We labeled the gaps with their Chern number. The obtained sequence of the Chern numbers in the spectrum in the low limit of $\frac{t_1}{t_0}$ is 1, 2, -2, -1, 0, 1, 2, -2, -1. It is within the expectations for two square lattice butterflies. In the upper limit, the Chern number sequence is 1, 2, 3, -1, 0, 1, -3, -2, -1. It is identical with the sequence obtained from the honeycomb lattice energy spectrum. The eighth-thirds band and seventh-fourth bands touch and split while Chern numbers are exchanged. The main central gap closes at $\frac{t_1}{t_0} = \frac{1}{2^{1/5}}$.

of bands at a particular flux $\Phi = p/q$ is $2q$ for two square lattice Hofstadter butterflies on top of each other, while it is $2q - 1$ for the honeycomb butterfly. It means, no matter how many closings and reopenings of energy bands happen, the number of these topological changes must be equal to each other except the central gap closing for the honeycomb structure. One interesting observation for band touching and splitting is the transfer of Chern number, but the total Chern number is conserved during this process. The evolution of the bands for $\Phi = \frac{1}{5}$ as a function of $\frac{t_1}{t_0}$ is plotted in Fig.5.6. As we reach the first closing in the spectrum, the sequence of Chern numbers of the gaps is 1, 2, -2, -1, 0, 1, 2, -2, -1

where the Fermi energy of the gaps is in increasing order. It is substituted with a sequence 1, 2, 3, -1, 0, 1, -3, -2, -1 when reach the honeycomb spectrum region, where $\frac{t_1}{t_0} = 1$. The central gap closes at $\frac{t_1}{t_0} = \frac{1}{2^{1/5}}$, and the eighth(third) band and seventh(fourth) bands touch and split while Chern numbers are exchanged at $\frac{t_1}{t_0} = 0.5$. Another example is for $\Phi = \frac{1}{13}, \frac{5}{13}$ in Fig.5.7. Bands can touch and split more than once depending on the denominator q. In the low limit of t_{10}, there are $2q$ bands for the two stacked square lattice Hofstadter butterflies. On the other limit, there are $2q - 1$ bands for the honeycomb Hofstadter butterfly. The Chern number sequences at both limits are known and must transform into another during the evolution. Thus, the Chern number transfers become essential during the transition.

Coming back to the experiment in Ref.[12], we can easily check to what extent the experimental setup realizes graphene under finite magnetic field. It can be shown that the q values greater than 8 in experiment are different from graphene. It is because the main gap is open for $q \geq 8$ in the experimental system while it is closed for all q values in honeycomb lattice. As long as the resolution of energy probes are not less than the width of the gaps (almost one percent of the full energy band width), the energy spectra of experiment and graphene are consistent with each other. It is possible to investigate the Chern number transfer adiabatically. The optical lattice can be arranged with various $\frac{t_1}{t_0}$ ratio as in Ref.[12], with a constant magnetic field as it was done in Ref.[4]. The adiabatic change of the optical lattice parameters can connect the checkerboard lattice gaps to the honeycomb lattice energy gaps, and the Chern numbers for large gaps can be measured.

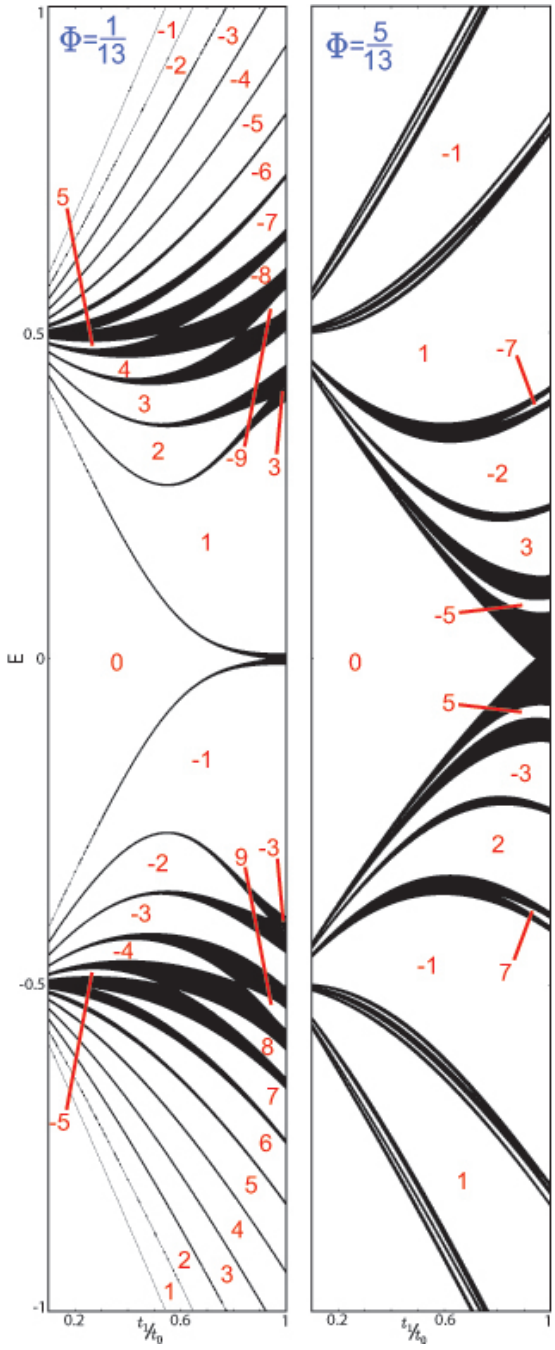

Figure 5.7: The evolution of bands for flux values $\Phi = 1/13, 5/13$ from the checkerboard to the honeycomb regime as a function of $\frac{t_1}{t_0}$. Bands can touch and split more than once depending on the denominator q. The Chern number sequences at both limits need to be connected obligatorily. Thus, the Chern number transfers are essential throughout the transition. Notice that Chern numbers not labeled for smaller gaps for visual clarity.

Chapter 6

Conclusion and Future Work

Demonstration of an artificial uniform magnetic fields in an optical lattice opens up a new area where it is possible to observe the Hofstadter butterfly energy spectra with cold atoms. This fractal spectra is determined completely by the lattice geometry and the applied field. The adjustable optical lattice created by the Zurich group lets the study of the Hofstadter butterflies for different lattice geometries.

This thesis aimed to investigate the evolution of the Hofstadter butterfly and its dependence upon the adiabatically changing lattice geometry in a periodic potential. A lattice geometry is defined by two properties: The primitive vectors for the Bravais lattice and the basis vectors in each unit cell. We examined the transition from the checkerboard to the honeycomb geometry, which indicates the change of basis vectors and keeping the primitive vectors constant.

Instead of going into the calculations for the main research, we first step-by-step calculated and discussed the Hofstadter butterflies for the square lattice and honeycomb lattice, which are essential for theoretical background. Starting from continuous exact Schrödinger equation, we approximated the system with the nn Tight-Binding Hamiltonian. Next, Peierls substitution is used to include the effect of magnetic field on the system. The energy difference equation was

obtained with the aid of Bloch theorem. It gives $q \times q$ matrix equation, and qth order characteristic polynomial. Then, we utilized the periodicity of the characteristic polynomial to greatly reduce the computation time for obtaining the Hofstadter spectrum.

After the theoretical background is provided, we calculated the self-similar spectrum for experimentally obtainable lattice parameters[3]. The results show that it is possible to examine the evolution of the energy spectrum for the transition from two square lattice butterflies with a large gap to the honeycomb lattice energy spectrum if a uniform magnetic field is generated on the tunable optical lattice in Ref.[3, 12]. The largest skeleton gaps except the central gap remains open during the transition process. However, the central gap disappears with the sequential touching of adjacent bands around zero energy. We found an analytical formula for the critical t_1/t_0 ratio where the Dirac point emerges for each $\Phi = p/q$ as $\left(\frac{t_1}{t_0}\right)_c = \frac{1}{2^{1/q}}$.

Another important result is that one cannot simply guarantee the Dirac points under finite magnetic field for the honeycomb lattice even if the Dirac points exist for zero field. The closer the $\frac{t_1}{t_0}$ is to 1, the more the energy spectrum of the Hofstadter butterfly is similar to the honeycomb lattice butterfly. Ideal honeycomb lattice spectrum and the experimental lattice spectrum become the same if $\frac{t_1}{t_0} = 1$. There are infinitely many closing and opening of minor energy gaps during the transition through which the Chern numbers are exchanged.

It is possible to investigate the Chern number transfer between neighboring bands, but these bands are so narrow compared to the width of the general energy spectrum, and the energy resolution may not be small enough to observe these closing and opening. That is why the artificial graphene demonstrated by the Zurich group can realize the honeycomb lattice Hofstadter butterfly[12].

As future work, we are planning to keep the basis vectors constant and change the primitive vectors arbitrarily, and examine the Hofstadter butterflies. Then, we can simulate the transition from one Bravais lattice to another, and examine resulting butterflies. We aim to combine the results and get a complete picture

about the dependance of the Hofstadter butterfly energy spectrum on lattice geometry.

Bibliography

[1] P. G. Harper, "Single band motion of conduction electrons in a uniform magnetic field," *Proceedings of the Physical Society. Section A*, vol. 68, no. 10, p. 874, 1955.

[2] D. R. Hofstadter, "Energy levels and wave functions of bloch electrons in rational and irrational magnetic fields," *Phys. Rev. B*, vol. 14, pp. 2239–2249, Sep 1976.

[3] L. Tarruell, D. Greif, T. Uehlinger, G. Jotzu, and T. Esslinger, "Creating, moving and merging dirac points with a fermi gas in a tunable honeycomb lattice," *Nature*, vol. 483, pp. 302–305, 2012.

[4] G. Jotzu, M. Messer, R. Desbuquois, M. Lebrat, T. Uehlinger, D. Greif, and T. Esslinger, "Experimental realization of the topological haldane model with ultracold fermions," *Nature*, vol. 515, pp. 237–240, 2014.

[5] I. Satija, "Topology and self-similarity of the Hofstadter butterfly," *ArXiv e-prints*, Aug. 2014.

[6] M. C. Geisler, J. H. Smet, V. Umansky, K. von Klitzing, B. Naundorf, R. Ketzmerick, and H. Schweizer, "Detection of a landau band-coupling-induced rearrangement of the hofstadter butterfly," *Phys. Rev. Lett.*, vol. 92, p. 256801, Jun 2004.

[7] S. Melinte, M. Berciu, C. Zhou, E. Tutuc, S. J. Papadakis, C. Harrison, E. P. De Poortere, M. Wu, P. M. Chaikin, M. Shayegan, R. N. Bhatt, and R. A. Register, "Laterally modulated 2d electron system in the extreme quantum limit," *Phys. Rev. Lett.*, vol. 92, p. 036802, Jan 2004.

[8] C. R. Dean, L. Wang, P. Maher, C. Forsythe, F. Ghahari, Y. Gao, J. Katoch, M. Ishigami, P. Moon, M. Koshino, T. Taniguchi, K. Watanabe, K. L. Shepard, J. Hone, and P. Kim, "Hofstadters butterfly and the fractal quantum hall effect in moiré superlattices," *Nature*, vol. 497, pp. 598–602, 2013.

[9] M. Aidelsburger, M. Atala, M. Lohse, J. T. Barreiro, B. Paredes, and I. Bloch, "Realization of the hofstadter hamiltonian with ultracold atoms in optical lattices," *Phys. Rev. Lett.*, vol. 111, p. 185301, Oct 2013.

[10] H. Miyake, G. A. Siviloglou, C. J. Kennedy, W. C. Burton, and W. Ketterle, "Realizing the harper hamiltonian with laser-assisted tunneling in optical lattices," *Phys. Rev. Lett.*, vol. 111, p. 185302, Oct 2013.

[11] R. E. Peierls *Z. Phys.*, vol. 80, p. 763, 1933.

[12] T. Uehlinger, G. Jotzu, M. Messer, D. Greif, W. Hofstetter, U. Bissbort, and T. Esslinger, "Artificial graphene with tunable interactions," *Phys. Rev. Lett.*, vol. 111, p. 185307, Oct 2013.

[13] Uehlinger, Thomas, Greif, Daniel, Jotzu, Gregor, Tarruell, Leticia, Esslinger, Tilman, Wang, Lei, and Troyer, Matthias, "Double transfer through dirac points in a tunable honeycomb optical lattice," *Eur. Phys. J. Special Topics*, vol. 217, pp. 121–133, 2013.

[14] D. Greif, T. Uehlinger, G. Jotzu, L. Tarruell, and T. Esslinger, "Short-range quantum magnetism of ultracold fermions in an optical lattice," *Science*, vol. 340, no. 6138, pp. 1307–1310, 2013.

[15] F. D. M. Haldane, "Model for a quantum hall effect without landau levels: Condensed-matter realization of the "parity anomaly"," *Phys. Rev. Lett.*, vol. 61, pp. 2015–2018, Oct 1988.

[16] R. O. Umucalılar and M. O. Oktel, "p band in a rotating optical lattice," *Phys. Rev. A*, vol. 78, p. 033602, Sep 2008.

[17] F. H. Claro and G. H. Wannier, "Magnetic subband structure of electrons in hexagonal lattices," *Phys. Rev. B*, vol. 19, pp. 6068–6074, Jun 1979.

[18] Rammal, R., "Landau level spectrum of bloch electrons in a honeycomb lattice," *J. Phys. France*, vol. 46, no. 8, pp. 1345–1354, 1985.

[19] J. Zak, "Magnetic translation group," *Phys. Rev.*, vol. 134, pp. A1602–A1606, Jun 1964.

[20] F. Yılmaz, F. N. Ünal, and M. O. Oktel, "Evolution of the hofstadter butterfly in a tunable optical lattice," *Phys. Rev. A*, vol. 91, p. 063628, Jun 2015.

[21] Y. Last, "Zero measure spectrum for the almost mathieu operator," *Communications in Mathematical Physics*, vol. 164, no. 2, pp. 421–432, 1994.

[22] R. O. Umucalılar, H. Zhai, and M. O. Oktel, "Trapped fermi gases in rotating optical lattices: Realization and detection of the topological hofstadter insulator," *Phys. Rev. Lett.*, vol. 100, p. 070402, Feb 2008.

[23] For animated evolution of the Hofstadter butterfly see Supplemental Material at link.aps.org/supplemental/10.1103/PhysRevA.91.063628.

[24] L.-K. Lim, J.-N. Fuchs, and G. Montambaux, "Bloch-zener oscillations across a merging transition of dirac points," *Phys. Rev. Lett.*, vol. 108, p. 175303, Apr 2012.

[25] D. J. Thouless, M. Kohmoto, M. P. Nightingale, and M. den Nijs, "Quantized hall conductance in a two-dimensional periodic potential," *Phys. Rev. Lett.*, vol. 49, pp. 405–408, Aug 1982.

[26] J. E. Avron, D. Osadchy, and R. Seiler, "A topological look at the quantum hall effect," *Physics Today*, vol. 56, p. 38, 2003.

[27] M. Aidelsburger, M. Lohse, C. Schweizer, J. T. Atala, M.and Barreiro, S. Nascimbène, N. R. Cooper, I. Bloch, and N. Goldman, "Measuring the chern number of hofstadter bands with ultracold bosonic atoms," *Nature Physics*, vol. 11, pp. 162–166, 2015.

[28] A. Dauphin and N. Goldman, "Extracting the chern number from the dynamics of a fermi gas: Implementing a quantum hall bar for cold atoms," *Phys. Rev. Lett.*, vol. 111, p. 135302, Sep 2013.

[29] D.-L. Deng, S.-T. Wang, and L.-M. Duan, "Direct probe of topological order for cold atoms," *Phys. Rev. A*, vol. 90, p. 041601, Oct 2014.

[30] W. Ketterle, "Inside the quantum hall effect," *Nature Physics*, vol. 11, pp. 90–91, 2015.

[31] H. M. Price and N. R. Cooper, "Mapping the berry curvature from semiclassical dynamics in optical lattices," *Phys. Rev. A*, vol. 85, p. 033620, Mar 2012.

[32] P. Středa, "Theory of quantised hall conductivity in two dimensions," *Journal of Physics C: Solid State Physics*, vol. 15, no. 22, p. L717, 1982.

Appendix A

Single Particle Numerical Schrödinger Equation in Periodic Potentials

We consider the single-particle spectrum in a two-dimensional periodic potential under a magnetic field perpendicular to the lattice plane. When the magnetic field is strong enough so that the flux passing through a cell is proportional to flux quantum h/e, it must be included into the Hamiltonian directly. The effect of the magnetic field is basically to introduce spatially dependent tunneling rates between neighboring sites which can be implemented to tight-binding Hamiltonian via Peierls substitution [11]. The exact diagonalization of the Hamiltonian is carried out by Nur Ünal.

In this work, in order to administer one-to-one correspondence to experiments, we start with the single-particle Hamiltonian without the magnetic field.

$$\mathcal{H} \;=\; -\frac{\hbar^2}{2m}\left(\frac{\partial^2}{\partial x^2}+\frac{\partial^2}{\partial y^2}\right)+V(x,y),$$

where for $V(x,y)$ we use the potential created by Zurich group,

$$V(x,y) = -V_{\overline{x}}\cos^2(kx+\frac{\theta}{2})-V_x\cos^2(kx)-V_y\cos^2(ky)-2\alpha\sqrt{V_xV_y}\cos(kx)\cos(ky)\cos(\varphi),$$

$k = 2\pi/\lambda$ is the wave vector where λ is the wavelength of the laser. α is the visibility of the interference pattern, the phases $\theta = \pi$ and $\phi = 0$ are set to the experimental values accordingly.

Exact Schrödinger eigenvalue equation is,

$$\begin{aligned}
\hat{H}|\Psi\rangle &= E|\Psi\rangle \\
\langle x|\hat{H}|\Psi\rangle &= E\langle x|\Psi\rangle \\
\Big[-\frac{\hbar^2}{2m}\big(\partial_x^2 + \partial_y^2\big) &+ V(x,y)\Big]\psi(x,y) = E\psi(x,y) \\
\Big[-\frac{\hbar^2}{2m}\big(\partial_x^2 + \partial_y^2\big) &- V_{\bar{x}}\cos^2(kx + \frac{\theta}{2}) - V_x\cos^2(kx) - V_y\cos^2(ky) \\
&- 2\alpha\sqrt{V_x V_y}\cos(kx)\cos(ky)\cos(\varphi)\Big]\psi(x,y) = E\psi(x,y).
\end{aligned}$$

The first job is to rotate the coordinate system by $\pi/4$ to be consistent with the experiment.

$$\begin{aligned}
x' &= \frac{x+y}{\sqrt{2}} \\
y' &= \frac{-x+y}{\sqrt{2}}.
\end{aligned}$$

The equation is made dimensionless. $\tilde{x} = x'/l$, $\tilde{y} = y'/l$, $\tilde{q} = ql$, $\tilde{E} = \frac{E}{h^2/2ml^2} = E/E_R$ and $\tilde{V_0} = \frac{V_0}{h^2/2ml^2} = V_0/E_R$, where $E_R = \frac{h^2}{2ml^2}$ is recoil energy. $l = \lambda/\sqrt{2}$ is optical lattice constant and set as the length scale.

$$\begin{aligned}
\tilde{E}\psi(\tilde{x},\tilde{y}) &= \\
&\Big[-\frac{1}{\pi^2}\big(\partial_{\tilde{x}}^2 + \partial_{\tilde{y}}^2\big) - \tilde{V}_{\bar{x}}\cos^2(\pi\tilde{x} + \frac{\theta}{2}) - \tilde{V}_x\cos^2(\pi\tilde{x}) - \tilde{V}_y\cos^2(\pi\tilde{y}) \\
&- 2\alpha\sqrt{\tilde{V}_x\tilde{V}_y}\cos(\pi\tilde{x})\cos(\pi\tilde{y})\cos(\varphi)\Big]\psi(\tilde{x},\tilde{y})
\end{aligned}$$

We need to approximate the partial derivatives, and then make the equation dimensionless. $\tilde{x} = n\Delta$, $\tilde{y} = m\Delta$

$$\begin{aligned}
\partial_x\psi(x,y) &\simeq \frac{\psi((n+1)\Delta, m\Delta) - \psi(n\Delta, m\Delta)}{\Delta} \\
&\simeq \frac{\psi_{n+1,m} - \psi_{n,m}}{\Delta} \\
\partial_x^2\psi(x,y) &\simeq \frac{\psi_{n+1,m} + \psi_{n-1,m} - 2\psi_{n,m}}{\Delta^2}
\end{aligned}$$

Rearranging the terms and defining $\Delta = 1/N$ where N is the number of points the dimensionless length 1 is divided into. Then, we get,

$$\begin{aligned}
\pi^2\Delta^2\tilde{E}\psi_{n,m} &= [4 - \pi^2\Delta^2 V_{\bar{x}}\cos^2(\pi n\Delta + \frac{\theta}{2}) + V_x\cos^2(\pi n\Delta) + V_y\cos^2(\pi m\Delta) \\
&+ 2\alpha\sqrt{V_xV_y}\cos(\pi n\Delta)\cos(\pi m\Delta)\cos(\varphi)]\psi_{n,m} \\
&- \psi_{n+1,m} - \psi_{n-1,m} - \psi_{n,m+1} - \psi_{n,m-1}.
\end{aligned}$$

$$\begin{aligned}
\pi^2\tilde{E}\psi_{n,m} &= [4N^2 - \pi^2(V_{\bar{x}}\cos^2(\pi\frac{n}{N} + \frac{\theta}{2}) - V_x\cos^2(\pi\frac{n}{N}) - V_y\cos^2(\pi\frac{m}{N}) \\
&+ 2\alpha\sqrt{V_xV_y}\cos(\pi\frac{n}{N})\cos(\pi\frac{m}{N})\cos(\varphi))]\psi_{n,m} \\
&- N^2\big(\psi_{n+1,m} + \psi_{n-1,m} + \psi_{n,m+1} + \psi_{n,m-1}\big)
\end{aligned}$$

It is time to apply Bloch condition to impose the periodic nature of wavefunction by a translation phase.

$$\begin{aligned}
\psi_{n+N,m} &= e^{i\vec{k}\cdot\vec{a}_1}\psi_{n,m} = e^{i\pi}\psi_{n,m} \\
\psi_{n,m+N} &= e^{i\vec{k}\cdot\vec{a}_2}\psi_{n,m} = e^{i\pi}\psi_{n,m}
\end{aligned}$$

The unit cell is divided into N^2 parts and the Bloch condition connects the boundary values. It is $N^2 \times N^2$ matrix equation, which must be diagonalized for each k_x, k_y pairs within the first Brillouin zone. Then, the lowest two energy values are what we are seeking for. Then, we implement a simple python code that calculates the optimum values for t_0 and t_1 for lowest two bands.